InfarctWatch: A Mobile Acute Myocardial Infarction Detection Service Using Commercial Smartwatch Electrocardiogram

University of Turku
Department of Technology
Master of Science (Tech) Thesis
Biomedical Engineering and Health Technology
May 2026
Janne Tyni

Supervisors:
Tero Koivisto
Jonas Sandelin

UNIVERSITY OF TURKU
Department of Technology

Janne Tyni: InfarctWatch: A Mobile Acute Myocardial Infarction Detection Service Using Commercial Smartwatch Electrocardiogram

Master of Science (Tech) Thesis, 78 p., 8 app. p.
Biomedical Engineering and Health Technology
May 2026

Many acute myocardial infarction patients do not seek medical attention early enough after they start to feel symptoms. Significant percentage of patients seek medical attention many hours after the infarction symptoms, worsening their prognosis. The reasons for the delay are complex in nature, but studies have found older age, first-time MI, lower income, symptom onset at night, underestimating symptom severity, fear of bothering others in a false alarm, and lower education level correlates with longer delay. This study implemented a system called InfarctWatch that enables patients to evaluate their commercial smartwatch ECG report for signs of myocardial infarction. Smartwatch is a common non-invasive piece of clothing accessory and is normal to wear in everyday life. This is why InfarctWatch works with smartwatches, to offer an inconspicuous service. InfarctWatch app will send the ECG report to server-hosted software called InfarctAPI. It extracts the ECG signal from the report with image processing techniques, preprocesses the extracted signal, and finally calculates features. These features are used to predict if the ECG contains signs of myocardial infarction with a trained machine learning model. InfarctWatch app displays the result and encourages patient to make immediate actions when needed. The model is trained using Lead I ECG signal from STAFF III database, consisting ECGs from 104 patients that are recorded before, after and during a balloon inflation procedure. This procedure effectively simulates ischemia and infarction, making this database essential for training MI detecting models. InfarctWatch is expected to function with any smartwatch model allowing its user to download the ECG report. For signal extraction, the drawn signal is expected to locate inside a grid. No integration development is done to any smartwatch, which requires InfarctWatch app to provide a robust, but in the end not very user-friendly solution for the user to upload their ECG file. Random forest model performed best with the test split resulting 0.912 accuracy, 0.947 precision, 0.9 recall, and 0.923 F1-score. The small scaled testing with 4 different smartwatches and 12 subjects resulted many false positives, due to how different in nature the training and extracted smartwatch ECG input data actually is. InfarctWatch did succeed well in extracting and processing the signal for ML prediction from the reports with a distinct visual design. The concept this mobile AMI detection system prototype demonstrates is considered impactful in making infarction patients seek medical attention earlier.

Keywords: Electrocardiogram, Machine Learning, Commercial Smartwatch, Myocardial Infarction, Mobile Application

Contents

List of Figures

List of Tables

List of acronyms

ACS Acute Coronary Syndrome

AI Artificial intelligence

AMI Acute Myocardial Infarction

ANN Artificial Neural Network

AUC Area under the curve

CV Cross validation

CVD Cardiovascular diseases

ECG Electrocardiogram

EMS Emergency Medical Service

FMC First Medical Contact

GUI Graphical user interface

HaH Hospital at Home

HF-ECG High-frequency electrocardiogram

HRV Heart Rate Variability

IHD Ischemic Heart Disease

LOO Leave-one-out

MI Myocardial Infarction

AMI Acute Myocardial Infarction

ML Machine learning

NN Nearest neighbor

NSTEMI Non-ST-Elevation Myocardial Infarction

PCI Percutaneous coronary intervention

PPG Photoplethysmography

RCT Randomized Controlled Trial

RL Reinforcement learning

RMSSD Root mean square of successive differences

ROC Receiver operating characteristic

SDRR Standard deviation of RR intervals

SE Structuring element

STEMI ST-Elevation Myocardial Infarction

TIT Total Ischemic Time

ML Machine Learning

1 Introduction

Cardiovascular diseases (CVD), including Myocardial Infarction (MI), are the leading causes of death globally [1]–[3]. MI prognosis gets worse the longer it takes to receive treatment after the onset of symptoms (Total Ischemic Time TIT) [4], [5]. To reduce myocardial damage, patients need to identify their symptoms and seek treatment as soon as possible. MI patients are usually over 60 years [6]. Older age is considered a risk group for many pathologies and requiring faster treatment in life-threatening situations [7]. Even patients that are well-informed about Acute Myocardial Infarction (AMI), can confuse their symptoms to other diseases they have already been diagnosed and medicated to. Atypical and even silent symptoms are also possible [8], making the situation more difficult for the patient.

Electrocardiogram (ECG) records the electrical activity of the heart in different viewpoints. Changes in peaks and segments of the ECG can indicate dysfunction in a specific area of the heart, and is therefore vital in the diagnostic process for cardiac conditions. In order to detect heart conditions faster, the ECG signal is also widely used in training machine learning (ML) models to predict MI [9], [10], atrial fibrillation [11], ischemia and heart failure [12]. Starting from 1950s, ML methods are used for making an artificial intelligence (AI) based system to emulate human decisions and actions, and the first AI application towards healthcare emerged in the 1970s [13]. Wearables have become increasingly popular due to health monitoring

and personalized wellness demands [14], [15]. Over one billion wearable devices are estimated to be used worldwide by 2028 [14], and 562 million smartwatch users count from 2025 is estimated to increase to 721 million by 2028 [15]. Ever since smartwatches with ECG sensors were released, the sensors' heart condition detecting capabilities have been studied considerably[10], [16]–[19]. Other health features that smartwatches and other wearables provide are: activity tracking (e.g. daily steps, running), heart rate, blood oxygen level, and sleep quality [16]. Before wearable health data, patient data were only collected after diagnosis or during physician visit. Now wearables can collect data from healthy and unhealthy, which can provide insights, enable detecting patient health risks, and predicting future outcomes.

Over the years medical systems have improved on giving AMI patients the required treatment faster, but it has no impact if the patient does not start the medical system process by contacting first. Many interventions for affecting patient behavior to AMI symptoms have been made (Appendix A). These interventions succeeded mostly in getting patients to call an ambulance and take aspirin, but not reducing the time it takes the patient to make contact after they experience AMI symptoms (patient delay). This thesis introduces another intervention: a decision support system called InfarctWatch, which works with any commercial smartwatch that has an ECG sensor. To have specialized equipment within your reach around the clock to save your own life can be considered stressful. Smartwatch however is a common non-invasive piece of clothing accessory that is normal to wear in everyday life, making the InfarctWatch inconspicuous for others and the patient itself.

InfarctWatch is a system that consists of 3 components: a commercial smartwatch, mobile application called InfarctWatch app, and a backend system called InfarctAPI. A prerequisite is that user is able to download their smartwatch ECG report to their phone. When patient is experiencing symptoms, first they measure their ECG

with their personal smartwatch. The ECG report is next downloaded from the smartwatch companion app. Patient sends the downloaded report to InfarctWatch app, which sends it to InfarctAPI for infarction evaluation. With image processing techniques InfarctAPI extracts the ECG signal from the report. The extracted signal is first preprocessed and then features are calculated for machine learning model prediction. The prediction is returned to InfarctWatch app, which displays the result and encourages patient to immediately call emergency number if needed. In addition, the app contains an info page that educates user about AMI symptoms and to call the emergency number if felt any symptoms recently, regardless if the symptom was not included in the page.

The background chapter 2 begins by first explaining heart anatomy, conduction, and circulation system in subsection 2.1.1. The action potential is discussed next in subsection 2.1.2 to introduce the basics of electrical activity between cells. Naturally next subsection 2.1.3 how these action potentials are measured with ECG. The smartwatch technological evolution and its remote healthcare capabilities are discussed in subsection 2.1.4. The definition, diagnostic process and treatment of MI is explained in section 2.2. The subsection 2.2.2 gives details about the AMI annotated ECG database that was used in ML model training. Finally, the main objective of the InfarctWatch to have an impact on, patient delay of MI patients is overviewed in subsection 2.2.1 by examining multiple studies to find out what interventions, common factors and how long is the delay in different countries.

The core concepts of machine learning and examples of its different methods and learning types are outlined in section 2.3. The fundamentals of image processing and its techniques that were used during the implementation is found in section 2.4. The implementation of InfarctWatch is described in chapter 3 by giving a brief architecture focused introduction. The section 3.1 explains the implementation process of

the mobile applications and its role in InfarctWatch. How the ECG was extracted from the report, ECG biomarkers detected, what features were calculated and how the model was trained is in section 3.2. The final results of the InfarctWatch is reported in chapter 4, its outcomes are discussed in chapter 5 and final conclusions are presented in chapter 6.

Generative AI tool has been used to give for help finding bugs from the InfarctWatch code, and as for the content of this thesis, there are cases where word suggestions for sentence has been asked, or suggestions how to rearrange too crowded sentences into multiple sentences. There are no code in InfarctWatch project or content in this thesis that is directly taken from the output of a generative AI tool. Some cited literature is found by a generative AI, but are of course reviewed before being included in this thesis. Most of the problems were already solved when writing the most detailed description about it to the tool. Explaining the problem in detail is known as rubber duck debugging in software engineering [20], but was also effective in other problems such as understanding some concepts in literature.

Thesis questions and hypotheses

To summarize, this thesis tries to find an answer to a question: (1) is it possible to build a decision support system functioning with commercial smartwatch ECG data, (2) could the service work as a third party service, and (3) could the service support multiple commercial smartwatch providers. The hypothesis is that it is possible to train ML model to detect AMI from smartwatch ECG, and enabling patient to detect AMI from home has significant impact on reducing the patient's delay on seeking the medical care they need to prevent death.

2 Background and key concepts

2.1 Heart

2.1.1 Anatomy and Physiology

The heart mostly consists of muscle tissue, located in the center of the chest behind the sternum, and contains 4 chambers. Upper chambers are called the left and right atria and lower chambers are called the left and right ventricles. These chambers provide blood flow to the circulatory system. This system is split into systemic and pulmonary circulation. Pulmonary circulation is the blood circulation between the heart and lungs, and systemic circulation is between the heart and the rest of the body. [21]

Chambers on the right side of the heart receives deoxygenated blood and pumps it to the pulmonary circulation for oxygenation (Figure 2.1). This starts in the right atrium, which collects deoxygenated blood from the systemic circulation. Once filled, the blood flows to the right ventricle through a tricuspid valve during atrial contraction. The right ventricle contracts to pump blood through the pulmonic valve to the pulmonary artery that distributes the blood to the lungs. Blood travels through capillaries that are located near alveoli (small air sacs) of the lungs where the oxygenation happens. Chambers on the left side of the heart receives the oxygenated

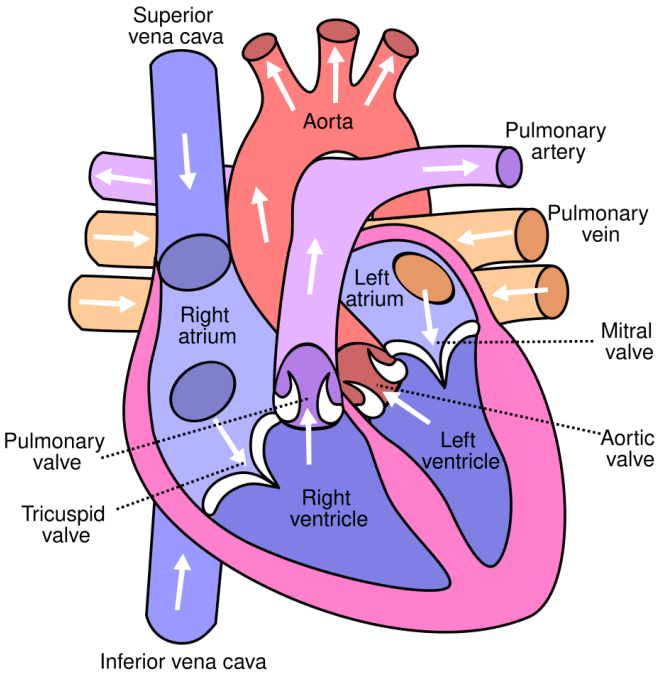

Figure 2.1: Diagram of the human heart. Arrows indicate direction of the blood flow. [22]

blood from pulmonary circulation and pumps it to the systemic circulation. This starts in the left atrium, which collects the reoxygenated blood from the lungs. After the atrium is filled, the blood then flows to the left ventricle through the mitral valve during atrial contraction. During ventricle contraction, the left ventricle pumps blood though the aortic valve to the aorta that distributes it to systemic circulation. Open valves only allow blood to move forward like described above and in normal conditions prevents backward flow [21].

The heart is made of three main tissue types: fibrous, electrical and contractile (Table 2.1). In skeletal muscle, the initial impulse comes from the nervous system. In heart, the stimulus comes from its electrical cells. The heart conduction system is formed by electrical cells, carrying electrical impulse to every part of the heart (Figure 2.2). The system also ensures that the contractions happen in the atria before the ventricles. The conduction system contains sinoatrial (SA or sinus node),

atrioventricular node, bundle of His, left and right bundle branches, and Purkinje fibres. Electrical impulse to heart muscle contraction, in other words the start of a heartbeat, is initiated by the sinus node. After the impulse has spread through the atria, the AV node delays the impulse to give atria time to finish emptying blood to ventricles. From AV node the impulse continues to His-Purkinje system, which carries the impulse to every part of the ventricles almost simultaneously, producing a rapid and effective contraction. SA node has the fastest depolarization rate (subsection 2.1.2), and if it deteriorates and slows down by age and/or disease, then AV node takes control. His-Purkinje system will take control if the AV node also deteriorates. The damaged conduction system may cause delayed, or completely missing ventricle contractions. [23]

Tissue type	Description
Fibrous	Support muscle mass, forms heart valves, does not contract and does not conduct electricity.
Electrical	Highly conductive, generate electrical impulses that trigger autonomic contraction, like a pacemaker.
Contractile	Most common type, contractions move blood through the heart.

Table 2.1: Main heart tissue types [23].

2.1.2 Action potential

Electrical activity in cells is based on their ability in regulating concentration of electrically charged electrolytes inside (cytosol) and outside (extracellular fluid) the cell membrane. The most important electrolytes in the heart are sodium (Na^+), potassium (K^+) and calcium (Ca^{2+}). Cell membrane has limited permeability to electrolytes. The permeability can be affected by opening and closing sodium-potassium pumps and ion channels in the membrane. At rest, the cytosol has a negative charge of approximately -90 mV when compared with the extracellular fluid charge. This electrical charge difference at rest is called a resting potential. [23]

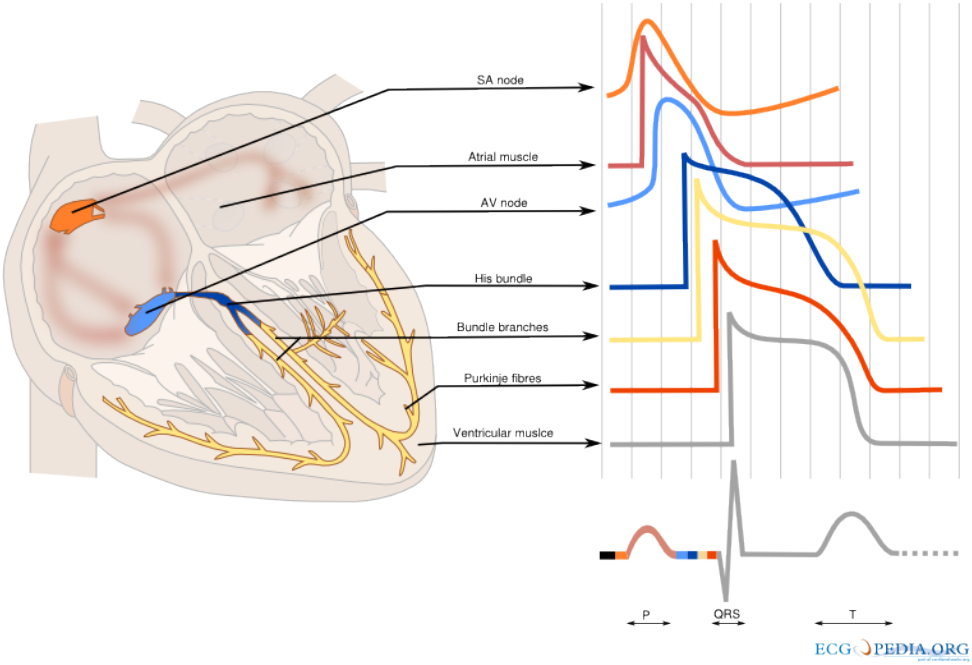

Figure 2.2: Heart conduction system and its components electrical activity during a heart beat [24].

When electrical impulse arrives at a myocardial cell membrane, the sodium channels open, allowing sodium to enter inside, which increases the charge inside the cell to slightly positive. The polarity with extracellular fluid changed, which is why this is called the depolarization phase. Once a cell has depolarized, the calcium channels open and calcium slowly enters the cell, which will stabilize the electrical charge, which then close the sodium channels. Calcium concentration increase in the cytosol triggers mechanical contraction. After the contraction, calcium channels close and potassium channels open and potassium flows out of the cell. This lowers cytosol electric potential, making it polarized again, which is why this phase is called repolarization. The process of cell depolarizing and later repolarizing is described as an action potential (Figure 2.3). After the action potential, the cell cannot be re-stimulated before it is near its resting state, which is called refractory period. This action potential spreads rapidly to adjacent cells and thanks to the refractory period

the same cell is not normally re-stimulated by the same action potential wave, which is why the propagation of the wave goes in one way until all cells are depolarized or meets non-conducting tissue. [23]

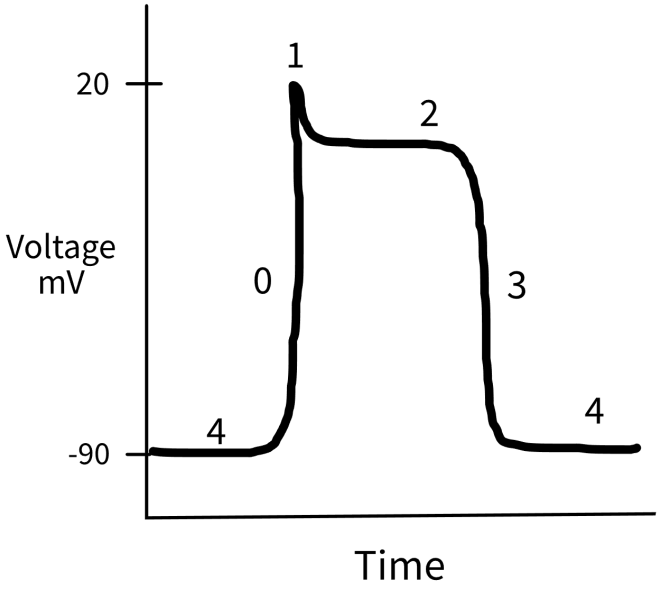

Figure 2.3: Representation of cardiac action potential with its phases explained [23]. 0: Sodium channels open and ions flow in; 1: depolarization, 2: Calcium channels open and ions flow in and contraction starts. Sodium channels close; 3: Repolarization, Calcium channels close, potassium channels open and ions flow out; 4. Resting potential. Only sodium-potassium pumps are active.

2.1.3 ECG

ECG records the of electrical activity from the heart in different viewpoints, and is vital data in the diagnostic process of cardiac conditions. It can provide the rate and rhythm of the heart, information about the health of the heart's electrical system, the size of the heart chambers, and myocardial blood supply. It is also useful in detecting non-cardiac pathologies like pulmonary emboli and electrolyte disorders. [25]

Standard 12-lead ECG records cardiac electrical impulses using 10 electrodes placed on the body, providing 12 leads. Each lead signal represents electrical activity

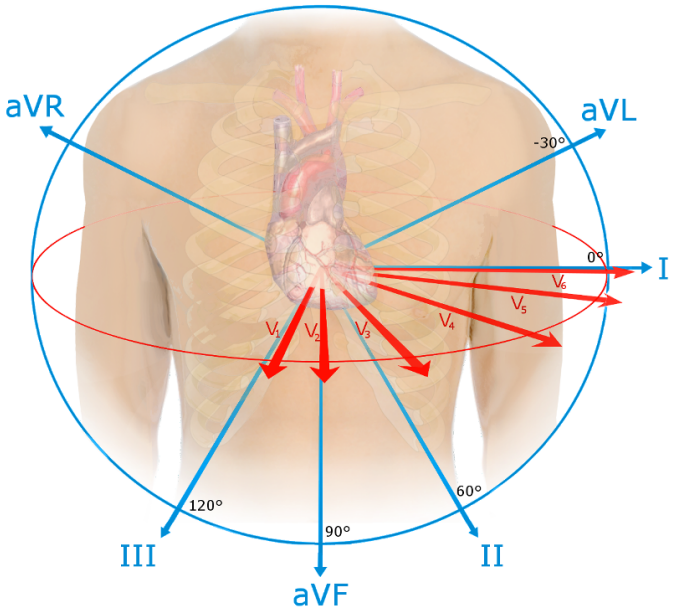

Figure 2.4: 12-lead ECG and the viewpoint of each lead visualized [26].

in different viewpoints (Figure 2.4) [23], [25]. Bipolar leads I, II and III are the standard limb leads (Figure 2.5). Their recordings are a sum between a positive and a negative electrode. For lead I, the positive electrode and negative electrode are placed on the left arm (+) and right arm (-) respectively, whereas for lead II, the electrodes are placed on the left leg (+) and the right arm (-), and finally lead III has its electrodes on the left leg (+) and the left arm (-). Unipolar leads are electrical potential records from one electrode (exploring electrode) paired with a ground electrode (indifferent electrode) that has approximately zero potential. The letter V is used for unipolar leads. Leads aVR, aVL and aVF are called augmented unipolar limb leads. The amplitude is augmented by 50% on these leads. The electrodes for these augmented unipolar limb leads are placed to the right arm, the left arm and the left leg respectively (Figure 2.5), effectively the same electrodes that are used for leads I, II and III. The remaining 6 leads (V_{1-6}) are unipolar and their exploring lead has a standard location on the left side of the chest. [25]

There are also special leads that are not part of standard 12 lead ECG. Posterior

chest wall positioned leads V_7 to V_9 can be useful for diagnosing STEMI, when ST segment depression is suspected from leads V_1 to V_3. Right precordial leads V_3R to V_6R are also useful for diagnosing right ventricular myocardial infarction. [25]

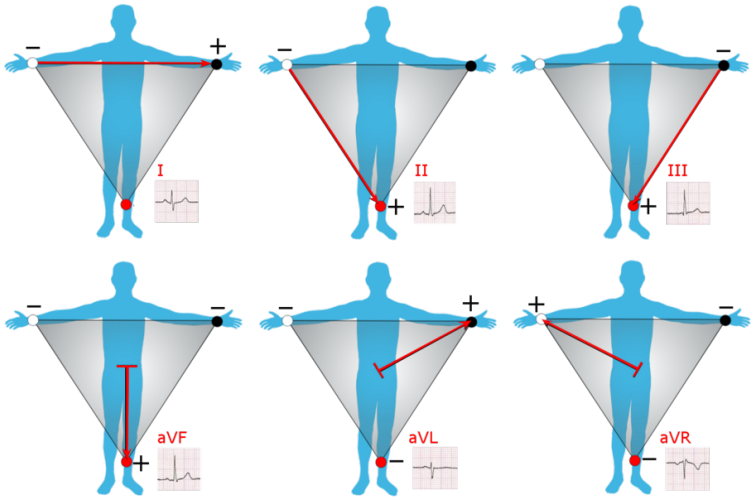

Figure 2.5: Bipolar limb leads I, II and III and augmented unipolar leads aVF, aVL and aVR [27].

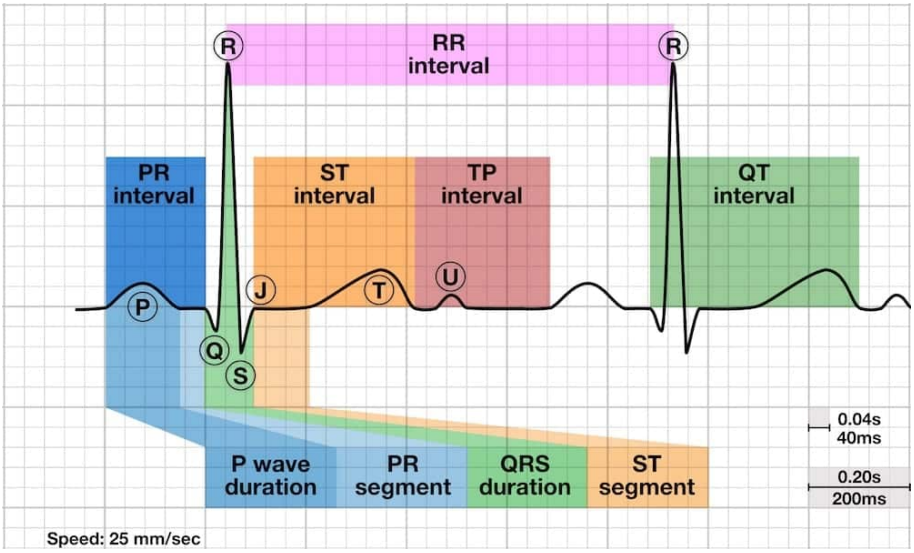

Figure 2.6: ECG waves, segments and intervals from heart beat [28].

In graphical representation of lead signals, the electrical activity that propagates towards the lead causes an upward waveform and propagation away from the lead causes downward waveform [29], [30]. During each heartbeat, the ECG shows a

sequence of waves: P, QRS complex, T, and sometimes a U wave (Figure 2.6). Recognizing abnormalities in shape, size, patterns and timings on these waves is the basis of ECG interpretation. Depolarization of the atria creates P wave, depolarisation of the ventricles creates the QRS complex, and repolarisation of ventricles creates T wave [23]. The origin of U-wave is uncertain [23], [28], [31]. The peaks, offsets and onsets of these waves are used to derive segments and intervals (Figure 2.6) for ECG interpretation (Table 2.2).

Metric	Description
ST-segment	Starts at J-Point (offset of QRS complex) and ends at onset of T wave. Represents ventricular refractory period before next simulation by repolarization. The segment is usually isoelectric (no electric charge changes) and any deviation is considered abnormal [25]. This interval is essential in the MI diagnostic process [32].
PR-interval	Start of P-wave to start of QRS complex [25], [30]. Represents time required for sinus impulse to activate atrium and travel to ventricles [25]. Useful for evaluating heart rhythm [30].
QT-interval	Onset of QRS complex to the end of T wave. Represents ventricular depolarisation and repolarisation process. [30]
R-R interval	Time between 2 consecutive R peaks. Used to estimate heart rate [30]. Fluctuation in RR interval times represent Heart Rate Variability (HRV).

Table 2.2: ECG segments and intervals explained.

2.1.4 Smartwatch ECG

Wearable smart devices have become popular due to increasing demand for health monitoring and personalized wellness [14], [15]. Over one billion wearable devices are expected to be in use globally by 2028 [14], and 562 million smartwatch user count from 2025 is estimated to increase to over 721 million by 2028 [15].

Köhler, Bartschke, Fürstenau, *et al.* [16] made a comprehensive study of smartwatch value in health sector, and its technological advancements (Figure 2.7). They categorized smartwatch use in health care into 3 domains: monitoring, nudging,

and predicting. Monitoring provides patient data during medical treatment and outside clinical facilities, giving supplemental insight to healthcare professionals. Nudging refers to a domain, where smartwatch is used to encourage individuals towards healthier behaviors by actively self tracking their health and fitness. Before smartwatch health data, patient data were only collected after diagnosis or during physician visit. Now smartwatches can collect data from healthy and unhealthy, which can provide insights to enable detecting patient health risks and predicting future outcomes.

Smartwatches include different sensors such as gyroscopes, magnetometers, barometers or altimeters, GPS, photoplethysmography (PPG) and ECG to gather data. Smartwatch manufacturer transforms this data into health features with their own algorithms, and the results are then shared to the user in a companion app, which is a smartphone application made by the manufacturer. Health features that smartwatches and other wearables provide are: activity tracking (e.g. daily steps, running), heart rate, blood oxygen and sleep quality, and ECG [16]. Since smartwatches with ECG sensors were released, its capabilities to detect heart conditions has been researched considerably [10], [16]–[19].

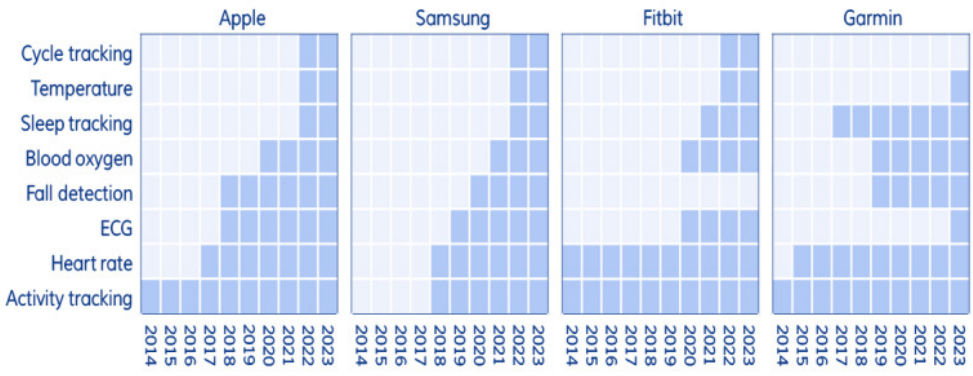

Figure 2.7: Evolution of health features across 4 leading smartwatch brands [16].

Medina-Avelino, Silva-Bustillos, and Holgado-Terriza [17] studied diverse sources to form a holistic understanding of the limitations and potential of wearable ECG de-

vices in home use. They investigated how wearable devices compare to 12-lead ECG, and what challenges in home use wearable ECG applications would bring. Various cardiac condition AI algorithms were also examined, and their advantages and challenges were discussed. They concluded that more research is still needed to make wearable ECG devices widely used in hospital at home (HaH) setting. Specifically these topics needs more research: advanced noise cancellation and signal processing, clinical validation of wearable ECG signals to make proper approximation, seamless compatibility with electronic health records and clinical workflow, and finally robust frameworks for data governance, privacy, and security. Leong, Lim, and Lai [33] reviewed ten HaH reviews, concluding that HaH generally provides similar or better clinical outcomes, shorter length of stay, and higher patient satisfaction compared to inpatient care. However, they also concluded due to low-quality evidence that the cost of HaH programs needs more clarification, and more evidence related to caregiver outcomes and adverse events in HaH care.

Diagnosing atrial fibrillation with smartwatch ECG is well established, but accurately detecting MI is currently considered requiring ECG data from various spatial locations to record multiple lead signals [10], [17], [18]. Therefore, the challenge with smartwatch ECG for MI detection is the limited lead capability where lead I is most common [17]. Figure 2.9 demonstrates how different leads can be measured with smartwatch and subsection 2.1.3 explains the leads more in depth.

Han, Song, Lim, *et al.* [10] had a primary goal to develop ML model that could detect AMI from sequential smartwatch ECG measurements from different leads. Secondary goal was to determine the minimum number of leads for sufficient detection performance. Model performance was compared to a commercial ECG analysis software from GE. The training data was based on 12-lead ECG records which were recorded within 24 hours of the visit. The recordings were then rearranged to emu-

Figure 2.8: ECG wearables: (**a**) from left to right, FitBit Sense, Apple watch series 4, Samsung Galaxy Watch 4 and Withings ScanWatch; (**b**) the Withings body scan is a smart scale that displays ECG data acquired via a multi-electrode grip (6-lead); (**c**) small, portable, medical-grade personal ECG device from AliveCor; (**d**) ECG patch for continuous monitoring. [17]

late as if they were measured asynchronously. As a result, they found that at least three leads are needed for a favorable model performance (AUROC 0.845, SD 0.011, single-lead sets: AUROC 0.768, SD 0.001).

Vries, Zepeda-Echavarria, Leur, *et al.* [34] tested their developed device prototype called miniECG on 8 pigs. The pigs underwent occlusion and reperfusion in anesthetic state, while the miniECG and 12-lead ECG recorded their heart activity. The ECG recordings were captured before, during and after occlusion, and the signals were then analyzed. MiniECG captured high quality ECG signals, and ST segment deviations were early detectable during the occlusion period. MiniECG is portable device that uses dry electrodes. It is operated via companion app that is installed

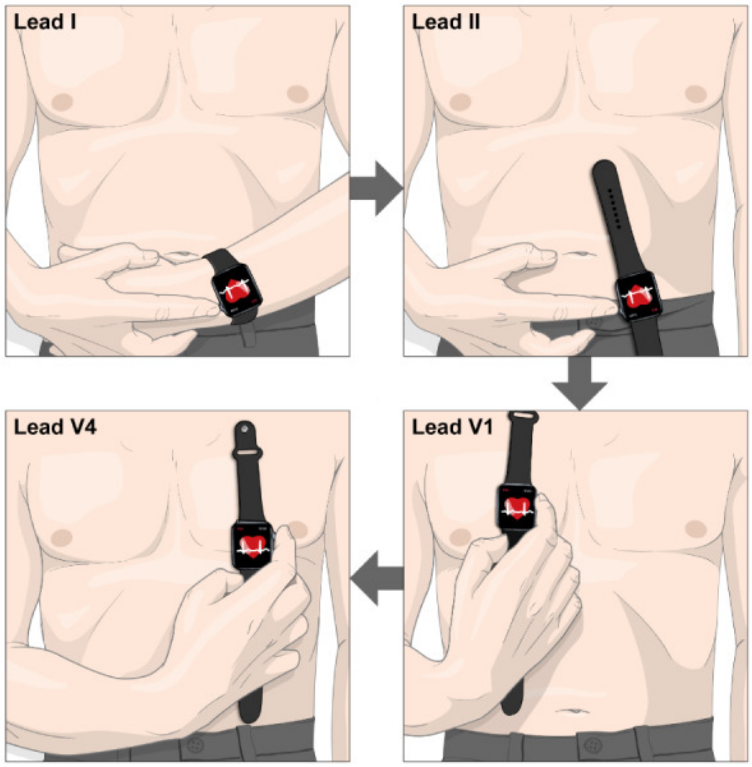

Figure 2.9: Examples how to measure different leads with smartwatch [10].

to a paired smartphone. This device is designed to be easy to use by patients when ischemic symptoms occur at home. The app would make immediate assessment of the captured ECG, and advise the patient next appropriate actions. Next step of development is clinical validation with human AMI patients. Monitoring, ambulatory, remote care, and integration with wearables and AI, were also seen as potential use of miniECG in the future. [34], [35]

2.2 Myocardial Infarction

Cardiovascular diseases are the leading cause of mortality globally [1]. Within CVDs, ischemic heart disease (IHD), which includes AMI, accounts for the largest share of deaths [2], [3]. According to World Health Organization [1] in 2022, 32% of global deaths were to CVDs (19.8 million people) and out of those deaths 85% were due to heart attack and stroke. Over the years, starting from 1990, the IHD mortality

rate has decreased thanks to improved health care [2]. Salari, Morddarvanjoghi, Abdolmaleki, *et al.* [36] estimated the global prevalence of MI in 2022 to be 3.8% among individuals that are younger than 60 years and 9.5% for aged 60 or more. High-income countries have a lower CVD mortality rate [1], [37]. The health care system differences between high- to lower-income countries is a prominent cause of mortality rate differences in CVD [1] and specifically in MI [38]. Unhealthy lifestyle is more common in developing countries [38], which affects the prominence of CVDs [1], [38]

MI is defined as necrotic myocardial cell death due to a prolonged lack of oxygen [32]. Myocardial ischemia is a condition where coronary flow in myocardial tissue is insufficient to the extent, when the tissue fails to sustain its level of cardiac performance that is required to support the physiological needs of the body [8]. In development of MI, myocardial ischemia is therefore the initial step [32]. It is commonly caused by coronary atherosclerosis, with or without superimposed thrombosis [8], [32]. Coronary atherosclerosis is lipid accumulation in artery wall (plaque) and inflammation of large arteries [39]. Thrombosis is a formation of thrombus (blood clot), which happens when the plaque from atherosclerosis erodes or ruptures, leading blood platelet activation and aggregation at the site [40]. Myocardial ischemia can also be caused by non-obstructive pathogenic mechanisms, like microvascular dysfunction or vasospastic disorders. [8]

Detecting myocardial injury by elevated cardiac troponin is a prerequisite to diagnose MI. Troponin elevation can also be a cause of other conditions, like myocarditis and renal failure. This is why abnormal cardiac biomarkers and evidence of acute myocardial ischemia are also required. Diminished ultrastructural myocardial changes are observable in 10 to 15 minutes after the onset of ischemia. Ischemic pain causing symptoms can occur in various combination in the chest, arms, jaw or upper

central abdomen. Fatigue and dyspnea are common non pain causing symptoms. These symptoms are not specific to ischemia only. Gastrointestinal, neurological, pulmonary, or musculoskeletal conditions also have these same symptoms. Atypical symptoms like palpitations and cardiac arrest, or even asymptomatic MI is possible [32].

ECG is essential to determine myocardial ischemia. Ischemic characteristics in ECG are ST-segment deviation from baseline, hyperacute T wave and T wave inversion in two contiguous leads. ST segment shift magnitude is determined with J-point (onset of ST segment) and onset point of the QRS complex. Pathological Q waves indicate myocardial necrosis, in other words MI. For proper treatment strategy for patient with acute coronary syndrome (ACS), the diagnosis of unstable angina or MI is needed first. If MI was diagnosed, it is then classified to either STEMI (ST-Elevation Myocardial Infarction) or NSTEMI (Non-ST-Elevation Myocardial Infarction). MI also has various types based on pathological, clinical and prognostic differences. [32]

STEMI contains a persistent ST-segment elevation on the ECG, and is usually an evidence of a complete occlusion in a coronary artery that requires immediate reperfusion therapy. NSTEMI does not have a significant ST-segment elevation on the ECG, which indicates that there is only a partial blockage or temporary disruption of blood flow in a coronary artery. If there is no significant ST-segment elevation, and biomarkers do not suggest there are myocardial injury, the patient is then diagnosed with unstable angina. [41]

Restoring normal myocardial blood flow is most important to stop further myocardial necrosis. Reperfusion therapy is an umbrella term for restoring blood flow and can be achieved in various medical (Table 2.3) and procedural ways [42]. Percutaneous coronary intervention (PCI), also known as angioplasty, is a procedure that uses a small balloon resembling instrument to reopen blocked arteries. A small,

Medication	Description
Anti-clotting	Aspirin and other blood-thinning medicines.
Nitroglycerin	Relieves chest pain and widens blood vessels to help blood pass the obstruction.
Thrombolytic medications	Clot-busting medication.
Antiarrythmia	Preventive medication for arrhythmia, which is a possible complication from MI.
Beta-blockers	Slowdown heart rate to improve heart recovery.
Antihypertensives	Decrease blood pressure and improve heart recovery.
Statins	For stabilizing plaque in arteries to reduce the chances of rupture. Reduce cholesterol and chances of having another heart attack.

Table 2.3: Possible AMI medications [42].

medication releasing tube called a stent is then placed on the site of blockage to keep the artery open. Door-to-balloon time is a metric that is an average time between patient arrival in the hospital and the start of the PCI treatment, and is commonly used in evaluating the medical service's efficiency to treat MI [42], [43]. Coronary artery bypass grafting (CABG), also called open-heart and bypass surgery, is another procedure for patients with severe blockages. Sternum is cut through in order to access the heart. The blockages are bypassed to bring oxygenated blood to the heart muscle. This is achieved by rerouting the blood flow using blood vessels from other sites like the chest, arm or leg [42], [44].

2.2.1 Patient delay

Reducing both patient and system delay are considered to be essential for lowering AMI in- and out-hospital mortality rates [45]–[47]. Shortening the patient delay however has proven to be challenging [47], [48]. On the other hand, since system delay has been more successfully improved over the years, the patient delay has become a much lower hanging fruit for reducing both treatment delay and total ischemic time [49], [50]. Patient delay as a metric has its challenges due to the bias of patients recall of symptom onset time. Symptoms can be ambiguous, meaning the

perceived first MI symptom might not be the actual first symptom. Other terms for patient delay are seen in papers as: decision time, and delay in seeking care. Other metrics that are used for measuring the overall delay of receiving care are also explained and discussed to give more holistic view about the patient delay.

Total ischemic time is the time between onset of symptoms to balloon or first device [47], [49], [50]. This time is observed in varying ways in studies. For example, it can be divided to patient delay and system delay (Figure 2.10). [46], [47], [51], [52]. Some studies use a metric called pre-hospital delay, that starts on the symptom onset, but when it ends varies: time of arrival to first medical contact (FMC), time of arrival to facility where treatment is done, or time when the treatment is given (Figure 2.10).

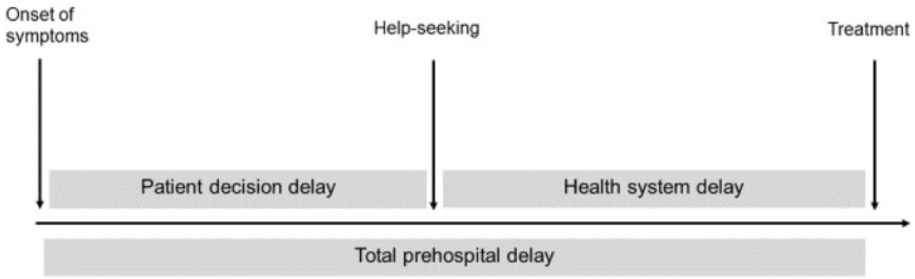

Figure 2.10: Prehospital delay where time of receiving treatment is defined as endpoint [53].

As shown in Table 2.4, the median patient delay is usually observed to be 90–240 minutes with varying IQR ranges and total ranges. The factors to this delay are complex, but there is evidence that older age, first-time MI, lower income, symptom onset at night, underestimating symptom severity and lower education level correlates to longer delays. Diabetes is also found to be an increasing delay factor for giving more atypical [59], [60], or even silent MI symptoms [60]. Female gender is often found as a relevant factor to patient delay [45], [56]. Some studies however have excluded gender as a relevant factor in their results [54], [55], [58].

Location (year)	Patients (n)	Patient delay (min)	Relevant factors	Author
France (2011–2012, 2016–2017)	481	Median: 87 (IQR: 36–216); Range: 0-1397	Age, FMC choice, Time of symptom onset	[54]
Korea (2014–2015)	350 (286 males, 64 females)	Males: Median 25; Range: 5–720; Mean: 49.4 (SD: 85.2) Females: Median 20; Range: 10–480; Mean: 59.2 (SD: 95.6)	Males: CVD history Females: Education level	[55]
Spain (2010–2013)	338 (76% males)	Median: 110 (IQR: 51–190)	FMC choice, Age, Gender, Diabetes	[56]
China (2012–2014)	3434 (77% males)	No patient delay specific metrics	Medical insurance, Perceived seriousness, Income	[45]
Denmark (1998)	337 (31% had AMI diagnose)	Median: 123; Non AMI median: 187; "silent" median delay: 60 (11–660)	Perceived seriousness, Self treatment	[57]
India (2017)	93 (81 males, 12 females)	Total range: 10–5450; Range: N patients 0–60: 35 61–120: 16 121–360: 21 361–720: 7 721–5450: 14	Pain intensity, chest pain presence, AMI knowledge, symptom perception, perceived seriousness, family support	[58]
Bangladesh (2017)	333 (67.6% males)	Median: 180 (IQR: 660)	Chest pain presence, Diabetes, Income	[59]

Table 2.4: Summary of relevant factors associated to patient delay in AMI from published studies. Year in parentheses indicates period of data collection in the study.

Rivero, Bastante, Cuesta, *et al.* [56] found that patients who made their FMC at home, were more likely to have long patient delay compared to patients who went directly to medical center. Caltabellotta, Magne, Salerno, *et al.* [54] discussed in their study how patient delay, pre-hospital delay and even system delay can grow significantly, if patient does not make their FMC by calling the emergency medical service (EMS). If patient first delay their FMC, and when finally taking action, chooses their FMC to be a facility that is unable to give proper treatment, are effectively suffering double penalty from their actions. Calling EMS from home should be therefore always the chosen FMC to minimize the overall delay to treatment.

Table 2.4 contains an older study from Denmark where the patient delay of chest pain patients were examined. They included a metric called "silent" delay, which is a time between symptom onset and time of consulting with nonmedical person. This was interestingly found to increase delay if the contacted person was a relative, but reducing when the person was non-relative. However, this was found among chest pain patients. It is unclear how relevant silent delay was for AMI patients since only 31% in the chest pain patient group had AMI diagnosed [57].

Wechkunanukul, Grantham, and Clark [6] made a global review of prehospital time for chest pain patients. After screening 338 studies they analyzed 23 of them, published from year 1996 to 2014. In total 153 811 participants were part of their review. The mean prehospital delay from these studies was 3.4 h ranging between 1.6 and 12.9 h. Seven studies had also reported the patient delay metric, and concluded it being a major component in prehospital delay. The ratio of the patient delay in the prehospital delay was ranging from 40.8% in Iran to 82.8% in Australia (Table 2.5). Old age, female gender, history of chronic disease and history of MI were the most common factors reported in the reviewed studies.

Caltabellotta, Magne, Salerno, *et al.* [54] studied how awareness campaigns impacts

Location (year)	Patients (n)	Patient delay (h)	Author
Saudi Arabia (2013)	189	Median: 2.5	[61]
Brazil (2014)	97	Mean: 0.94	[62]
Denmark (2004)	250	Median: 1.23; 69% of total delay	[63]
Iran (2012)	513	1; 40.8% of total delay	[64]
UK (2009)	228	53.7% of patients had patient delay $\leq$ 1; 60% of total delay	[65]
Australia (2005)	150	Mean: 2; 82.8% of total delay	[66]
China (2009)	498	1; 57.2% of patient had delay $\leq$ 2	[67]

Table 2.5: Patient delay reported from primary studies summarized by Wechkunanukul, Grantham, and Clark [6]

.

the patient delay. Core message in campaigns were "call fast, call 112". Campaign channels were newspapers, radio and television advertisements, billboards in main cities and newsletters to healthcare providers. The campaign was published first in 2013, and again in 2015. Patients choosing EMS as their FMC increased from 55% to 62% in 2016–2017 period, but there was no relevant change in patient delay when compared to 2011–2012 baseline period.

Banharak, Metprommarat, Mahikul, *et al.* [68] made a systematic review and meta-analysis on effectiveness of different interventions to AMI on selected outcomes. They reviewed 11 studies and were located in the USA and Germany. Older female adults were majority group on each study. A total of 8 categories were identified from these studies (Appendix A). Only calling to EMS and taking aspirin for chest pain improved on some interventions, which aligns with the findings of Caltabellotta, Magne, Salerno, *et al.* [54]. Teixeira, Zancaner, Ribeiro, *et al.* [69] made an intervention that utilized communication platform WhatsApp to enable patient send their ECG from home to medical professionals for AMI analysis. This intervention resulted to have positive impact in mortality, and percentage of patients who received therapy.

Another form of behavior change focused intervention was studied by Farquharson, Johnston, Williams, *et al.* [70]. They formed 3 groups from 145 volunteered patients who recently had experienced ACS. Only 8% of volunteered patients were diagnosed with MI. The intervention channel was a website, and it was experimented with a Randomized Controlled Trial (RCT). The randomized groups had varying forms of content displayed on the website: visual and text, text only and control group. Group who saw both text and visual content had usual care, 8 minute animated education video and interactive exercises. The content in text only group differed by replacing the video with its voice over in both audio and text format. Lastly, the control group only received usual care. Study results are based on before and after intervention questionnaire. The questionnaires were asking about patients intentions to act in different AMI related scenarios. The study concluded the content containing both text and visuals to possibly increase the intention of calling the ambulance immediately at the onset of ACS symptoms.

So far there are no real world ML based intervention to support AMI patients seek medical care faster at home. Real world interventions are mostly educational and promoting, like the previously mentioned studies. ML based patient delay interventions are not widely studied as the main objective, but is suggested as potential use case in form of automated AMI detection service [10], [71]. A distinct acknowledgement of the state of patient delay was in an article made by Zhao, Xiong, Hou, *et al.* [72]. They had a high emphasis about the potential impact of their 12-lead ECG based ML model towards patient delay in an auto diagnostic setting.

2.2.2 STAFF III database

This database consists of standard 12-lead ECG recordings with a sampling rate of 1000 Hz and was acquired in 1995 and 1996, where 104 patients had their ECG recorded before, during and after a prolonged balloon inflation. It was originally

made for analyzing ECG signatures during acute ischemia and especially focusing on high-frequency QRS components [73], but its use has broadened over the years to other research problems than high-frequency ECG (HF-ECG) analysis [74]. This prolonged balloon inflation reduces the blood flow of the heart muscle tissue, effectively simulating acute myocardial ischemia and infarction. Other studies have also used this database to make AMI analysis and ML models [9], [75], [76].

Pre-inflation ECGs were 5 minutes long at rest in supine position before any catheter insertion. The recordings were performed either in a patient's room or catheterization laboratory, or both. The ECG during inflation was captured once, or in some cases up to five times. The mean inflation time was 4 min 23 s, ranging from 1 min 30 s to 9 min 52 s. From the total of 152 occlusions, 58 were in left anterior descending artery, 59 in the right coronary artery, 32 in the left circumflex artery, and finally 3 in left main artery. Post-inflation ECGs were again 5 minutes long at rest in supine position in either patient's room or catheterization laboratory, or both. [73]

From this database, the first ECG recording session can be used as a baseline healthy ECG and compare it with an ECG during inflation. Also, the possible second pre-inflation can be used to compare with the first ECG to be able to consider the variation in the signal when measurement place, time, and to some extent, the electrode placement is different. This kind of comparison between ECG recordings from different times is called serial ECG, and it is an important procedure for MI detection among cardiologists [77]. There is evidence, that a serial ECG could be applicable for training machine (and deep) learning models to predict MI [9], atrial fibrillation [11], ischemia and heart failure [12].

2.3 Machine Learning

Machine learning (ML) is a tool to find statistically meaningful patterns from data. Pattern searching made by a machine learning model is useful in complex tasks where human cannot make themselves a detailed specification with program code to perform the required task. These kinds of tasks could be originally performed by humans such as driving, speech recognition and analyzing images. Data mining, which requires analyzing very large and complex data sets is another good example. [78]

Jung [79] split ML in his book into 3 basic components: data, model and loss. Data is a collection of data points sourced from varying representations like text, documents, signal, images, and videos. The amount of data points is preferably large for ML methods for more accurate predictions. Data points contain 2 different groups of properties that are relevant for making a prediction: features and labels. The feature group contains low-level properties of a data point that can be automatically computed or measured. Labels are higher level properties that represent a classifying fact or quantity of interest, which are associated with the features of the data point. Problems that require predicting classification or category labels are called classification problems, such as detecting cancer from medical image or identifying whether an email is actually spam. Problems that involve predicting numeric labels are called regression problems, such as forecasting weather temperature, house prices or age of death.

ML models do not actually learn, but instead finds the best hypothesis by calculating loss of each hypothesis and selects the one that gave the least loss. From a space of infinite hypotheses, different models have their own methods to select what hypotheses it includes in their own space, how the prediction loss is calculated, and what tunable hypothesis parameters are available. ML methods have been used since 1950s to make AI based systems for emulating human decisions and actions [13].

$$h^{(w)}(x) : \mathbb{R}^n \to \mathbb{R} : x \mapsto w^T x \tag{2.1}$$

Hypothesis h is in short a function that returns a predicted label based on the data point features. Each hypothesis have their own weighting for each feature. The weighting vector w contain numeric values which represents how much the features in vector x is associated to the true label (Equation 2.1). The hypothesis space $\mathcal{H}$ can be manipulated with the previously mentioned tunable parameters (Equation 2.2). These parameters essentially transform the features $\phi(x)$, which affects the performance of each hypothesis in the space and potentially the new best performing hypothesis is able to predict data point labels better, than the one before any parameters were tuned. [79]

$$\mathcal{H}' := h'(x) := h(\phi(x)) : h \in \mathcal{H} \tag{2.2}$$

2.3.1 Loss

If a model predicted correctly that an image of a single animal contains a zebra, but it was nearly as confident that the image contained an eagle, would the model be considered to have generalized well with its training data? How about a model that predicts person age, and there are near zero errors when person is in their 30s, but in any other age the prediction varies considerably? A model with minimal errors can give misleading performance results if different kinds of errors, like different magnitudes or inconclusive classifications are not handled properly.

The loss function L quantifies the dissimilarity between predicted $\hat{y}$ and true label y. Each data point is predicted by all hypothesis candidates. The hypothesis that resulted the least loss with all data points is selected. How the loss is calculated

can have significant difference what hypothesis performs the best. As an example for regression models, there are squared and absolute error loss functions.

$$L\big((x, y), h\big) := (y - \underbrace{h(x)}_{=\hat{y}})^2 \tag{2.3}$$

Squared error function (Equation 2.3), as its name implies, squares the error $y - \hat{y}$, causing predictions that are close to the true label accumulate less loss than predictions that are further. Compared to absolute error loss, which simply calculates the absolute difference between the predicted and actual value, the loss increases linearly based on the difference. The zero-one (0/1), hinge, and logistic loss functions are common with classification models. The 0/1 loss function adds zero loss on correct classification and one on incorrect classification (Equation 2.4).

$$L\big((x, y), h\big) := \begin{cases} 1, & \hat{y} \neq y \\ 0, & \hat{y} = y \end{cases} \tag{2.4}$$

As for hinge in binary classification, there is minimal loss for correct prediction that are confident. The loss increases based on the confidence value of the incorrect prediction. The logistic loss function on the other hand lowers the loss for correct predictions and raises it for incorrect ones based on the confidence value. In other words, logistic and hinge loss gives more loss to the hypothesis the more confident incorrect prediction, but logistic also reduces the loss the more confident correct prediction is. [79]

2.3.2 Supervised Learning

Supervised learning uses data points that has known true label. With given set of data points known as a training set, the supervised ML model finds a hypothesis that resulted the least loss with all given data points. Training set refers to a subset of available data that is used to train the model. Test set is the remaining set of available data points, and it is used to evaluate the general performance of hypothesis the ML model had selected with the training set. Already labeled data is manually done by human experts of the data points domain. There are even marketplaces for renting human workforce to label data. You could say that supervised ML tries to find a hypothesis that can imitate the same annotation behavior as humans with feature data only. [79]

2.3.3 Unsupervised Learning

There is also unsupervised learning, which does not have any label values. This kind of learning is finding hypothesis that are based on the features values only. For instance clustering methods, which finds groups that share similar data points. Also feature learning methods, which finds the most relevant features by constructing the original feature set dimensionality to another with minimal reconstruction error. In other words, feature learning changes the amount of features while trying to retain the same information, where the loss function is based on the difference of the original and reconstructed feature value. This is most commonly used for reducing feature set to improve overall computational time. Reducing feature set is also known as dimensionality reduction. [79]

2.3.4 Reinforcement Learning

Reinforcement learning (RL) is applied also into non labeled data like unsupervised ML, but its predictions influences the generation of future data points to make

predictions out of. RL applications involve data points that are at different time instants and represent a state of a system. For example self-driving car or playing chess. How is it possible to evaluate prediction loss of a car steering angle or chess move in one time instance to other predictions? Car cannot move left and right or in chess make 2 moves at the same time. Prediction also influences the future data. Once car has turned, the state of the system has changed in next time instance and another prediction is needed. State of the chessboard has changed after previously predicted move is executed. These kinds of problems require a reward signal that changes in the state, to better or worse, in order to evaluate the loss between previous state and current state influenced by previous prediction. For example a sensor to measure the distance between car and the described location. [79]

2.3.5 Nearest Neighbors

Nearest neighbor (NN) models predicts data point labels based on other similar data point label values. The similarity is determined by measuring a distance between other data points in feature space. Euclidean distance is commonly used to determine these distances. The label values are observed from the k nearest neighbors of the data point. The most prominent label among the neighbor labels is selected as a prediction in classification models. In regression, the predicted value is based on the average of the NNs label values. The tunable parameter k should be odd in classification to make sure the label values will not be evenly distributed. [79]

Two different k nearest neighbor classifier decision regions for iris flower species is shown in Figure 2.11. Unlike Versicolor and Virginica, notice how Setosa data points have almost perfect distinction from other decision regions with this 2 feature set: sepal length and width. Comparing the plots it is noticeable how the region complexity increases when k is much smaller by even making a small extra region for Virginica in Versicolor region. Training a well generalized model to unknown data is

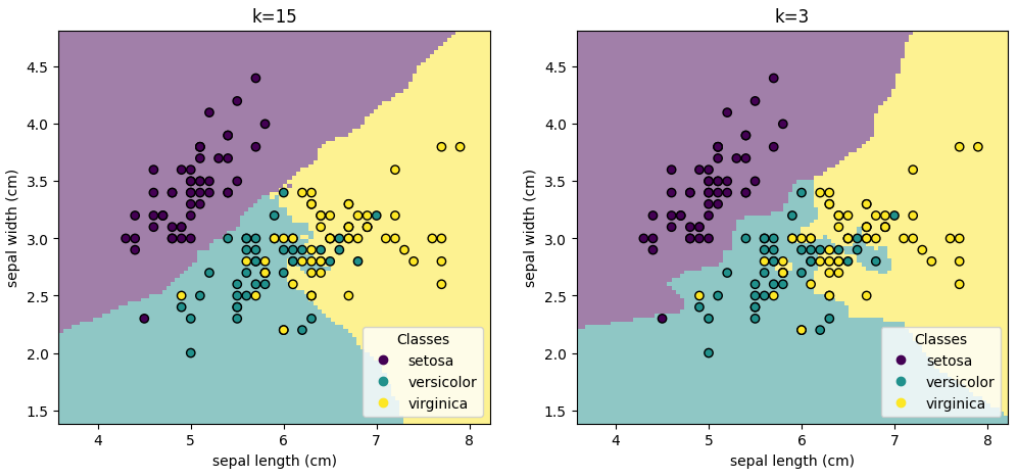

Figure 2.11: Decision boundaries of iris data set to predict specie with k nearest neighbor classifiers.

done by finding a good balance between over complex and too simple decision region. In this figure case, it could be assumed that these models with these features would generalize well with predicting Setosa, but not with the other species.

2.3.6 Decision Tree

Decision tree models test data point features in flowchart resembling manner. There are two kinds of nodes in the decision tree: test nodes which test features, and leaf nodes which is the end point of testing and corresponds to a label value to a subset of feature space. The next node is selected in the test node based on whether the feature test passes or not (Figure 2.12). These feature testing nodes essentially build decision boundaries in feature space (Figure 2.13). The leaf nodes give a specific label value based on these boundaries, forming something that resembles a decision region to this particular label. [79]

Using iris data as an example in Figure 2.12, the petal length is first tested in the first white test node. The model in this example was set to have only two depths for demonstration purposes. If test fails the next node will be the connected node

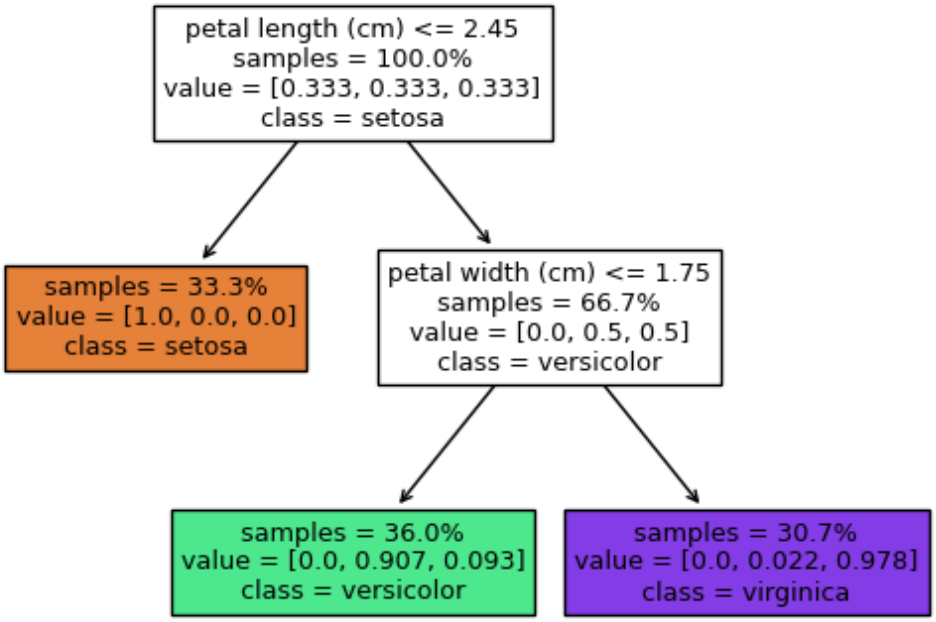

Figure 2.12: Structure of decision tree model to iris data with all features in training set. Maximum depth set to two to make structure simple.

on the left side of the tree, otherwise the connected node on the right side is next. For this iris case the data point is predicted as Setosa (orange leaf node) when its petal length > 2.45. If length test passes, meaning petal length ≤ 2.45, the petal width is next tested in white test node in next depth. The result of this second test determines data point's predicted class. When petal width ≤ 1.75, the data point is predicted as Virginica (purple leaf node), otherwise Versicolor is predicted. The value info in nodes represents the distribution of label values of data points that have reached the node in this order: Setosa, Versicolor and Virginica. At first node we can see that there are equal 33.3% distribution of data points for each label. In orange leaf node the first value is 1, meaning 100% of nodes that ended their pathing here were correctly classified as Setosa. In other leaf nodes however, there are classification errors: 9.3% of data points that ended up to green leaf node are actually Virginica and 2.2% of data points that reached purple leaf node are

Versicolor.

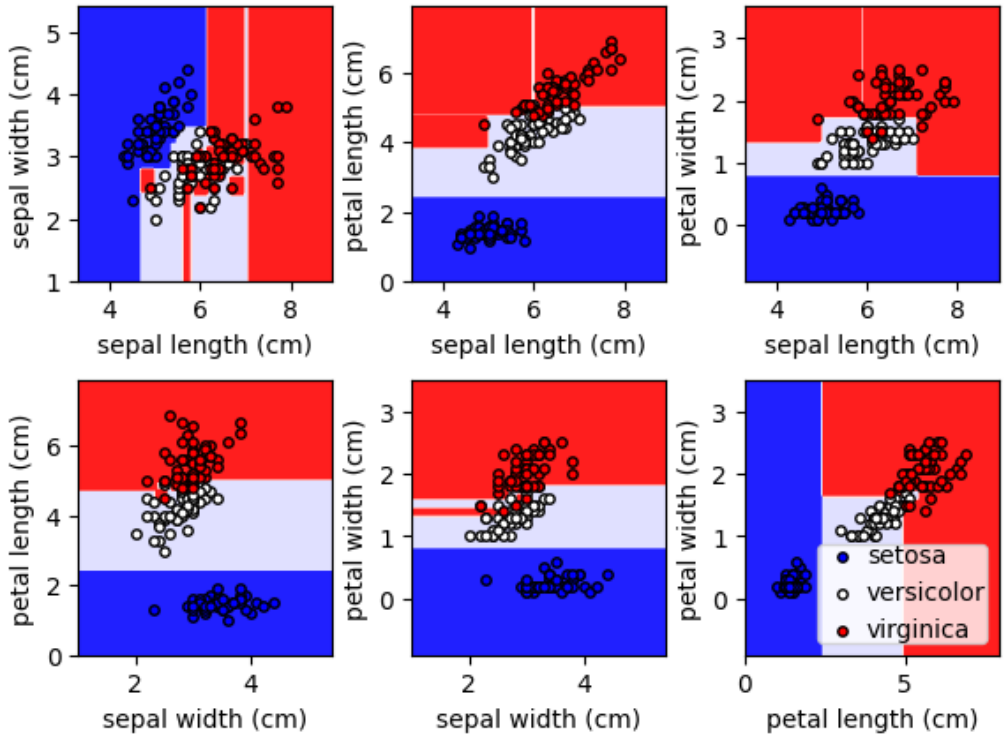

Figure 2.13: Decision boundaries of decision tree model with iris data using different combinations of two features in training.

2.3.7 Deep learning

Deep learning methods use artificial neural networks (ANN) to make predictions. These neurons produce new weightings to features by summating the weightings sent by other connected neurons. The connections to these neurons where they send or receive their weightings are arbitrary. A common approach to organize neurons and the connections for visualization is with layers (Figure 2.14). Neurons in layers are usually connected with neurons in consecutive layers. ANN with many layers is usually called a deep net, which is why ML methods that use deep ANNs are called deep learning methods. [79]

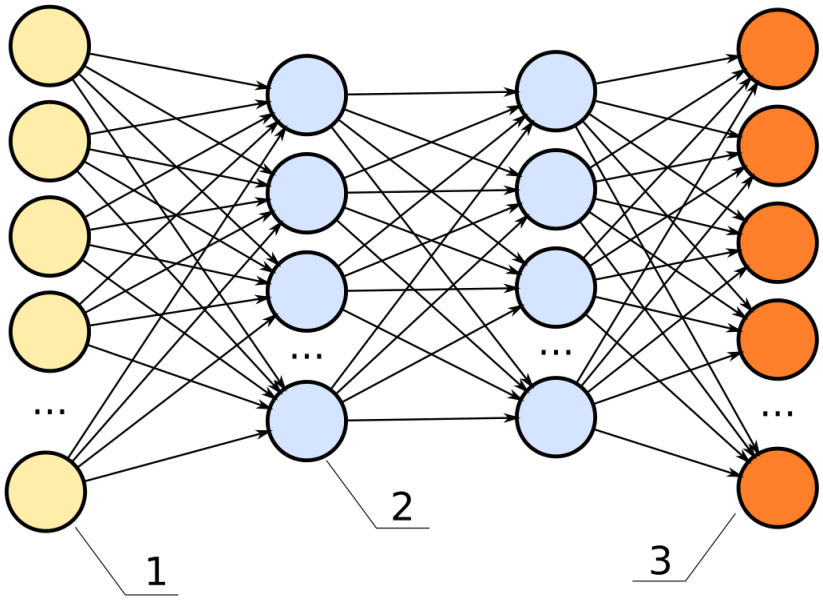

Figure 2.14: Example of a neural network visualized with layers: input layer (1), hidden layers (2) and output layer (3) [80].

2.4 Image processing

An image can be defined as a two-dimensional array, where the dimensions represent the (x, y) coordinates and the pixel value is accessed with function $f(x, y) = I_{x,y}$. The values correspond to the color intensity of the located pixel. The pixels in digital images can have a finite number of distinct intensity values and images are commonly referred as "k-bit images", meaning it can contain 2^k distinct intensity values. For example, an image that can contain up to 256 distinct values is an 8-bit image ($2^8 = 256$). Humans have a limited visual band in the electromagnetic spectrum. Digital image processing, which is built on mathematical and probabilistic formulations, can provide crucial additional information about the image with its much wider visual band. [81]

2.4.1 Unsharp masking

Unsharp masking is a common procedure to sharpen an image. It subtracts the blurred version of the image from the original, producing a mask image that contains the small details that were not blurred so effectively. To visualize these small details in its real context, the mask is then added with optional weighting k to the original image (Equation 2.5). [81]

$$f_{sharpened}(x,y) = f_{orig}(x,y) + k * (f_{orig}(x,y) - f_{blur}(x,y)) \tag{2.5}$$

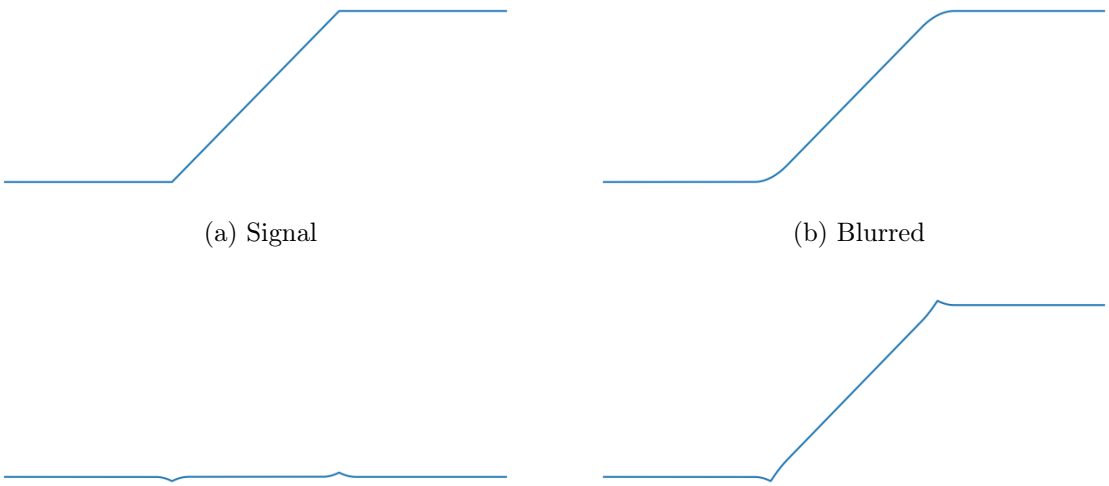

(a) Signal (b) Blurred

(c) Mask (d) Sharpened

Figure 2.15: Unsharp masking process illustrated with one dimensional signal.

Using one dimensional signal gives a simple example of how a color intensity change in an image would be affected by unsharp masking (Figure 2.15). Notice the sharp edges in Figure 2.15a which corresponds to the points where the intensity change starts from low and then stops at high. Moving average filter is used to blur the signal in Figure 2.15b, and as a result the sharp edges are smoothened. When the blurred result is subtracted from the original signal, only those sharp edges remain in the mask as noticeable intensity change. The mask was then added to the signal,

using k weighting of 1 (Equation 2.5), enhancing the signal at points the intensity change starts and stops.

2.4.2 Greyscaling

The color spectrum of visible light can be divided into six broad colors: violet, blue, green, yellow, orange, and red. Due to how human eye senses different wavelengths, it has been found that most (but not all) colors can be perceived as a combination of three primary colors: red, green and blue. The RGB color model is commonly used in digital images. This can be thought as a single RGB image actually having a red, green and blue color shaded images on top of each other with different intensity levels, resulting a distinct color for each pixel. Greyscaling simply means representing the intensity values of multicolor images, like the RGB image, as in one color instead. This can be achieved by simply taking one of the channels that has the most morphological information of interest, or by using a weighted sum of all available channels as shown in Equation 2.6. The colors are between black and white (Figure 2.16a) in a greyscaled image, and the higher the intensity value the brighter the pixel is. [81]

$$I_{grey} = I_{red}W_{red} + I_{green}W_{green} + I_{blue}W_{blue} \tag{2.6}$$

2.4.3 Image histogram

As mentioned before, each pixel intensity values are stored in an image file and can contain k-bits (2^k) different values. A histogram of an image shows how many pixels are in different intensities. As seen in Figure 2.16b, the majority of the pixels have intensity values larger than 225 in an 8-bit ($2^8 = 256$) image. Manipulating this histogram is a common procedure for image enhancement [81]. When for example

normalizing an image that has a narrow histogram, the distribution of different intensity values turns wider, which considerably increases the contrast of the image. In Figure 2.16 you can see this distribution change by comparing the histograms before (Figure 2.16b) and after equalization (Figure 2.16d), and how the image contrast increased between Figure 2.16a and Figure 2.16c.

(a) Greyscaled image

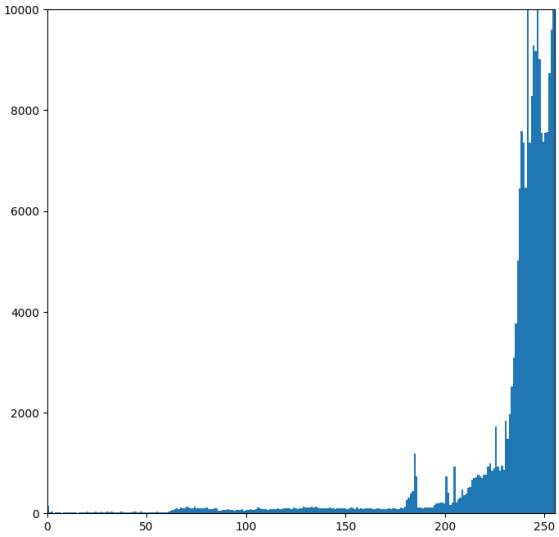

(b) Histogram of the greyscaled image

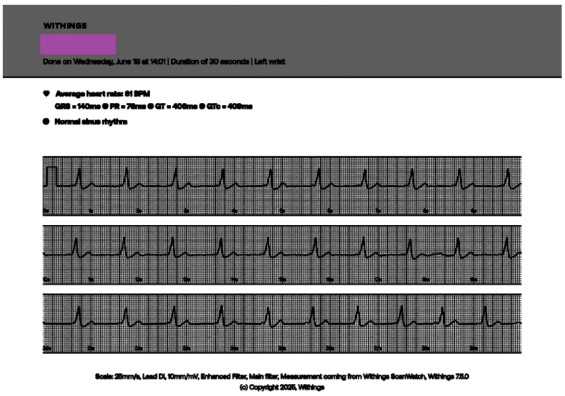

(c) Histogram equalized image

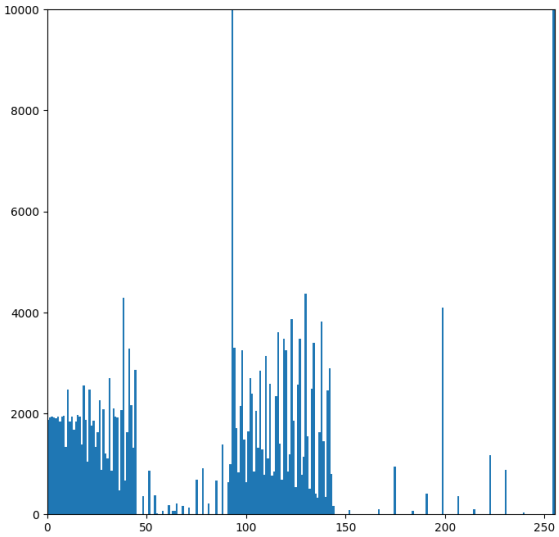

(d) Equalized histogram

Figure 2.16: Histogram equalization example with Withings smartwatch ECG report. Histograms are zoomed in order to better visualize the less frequent intensity distribution.

2.4.4 Binary image

Binary images only contain two intensity values 0 and 1, where the 0 (black) represents the background and 1 (white) the foreground of the image. What intensities in the image are considered as background or foreground depends on the task objective. The distinction can be done by setting a single or multiple intensity threshold points that define whether the pixel is considered background or foreground. The threshold could be selected manually from the image's histogram, or use an algorithm to determine the threshold automatically. For example, when inspecting the equalized histogram in Figure 2.16d, the vast majority of the lower intensities are below 150 in form of two clusters. The two clusters of darker pixels are divided between 50 intensity and brighter colors are over 150 intensity. Figure 2.17a is the result of choosing only the darker cluster in the histogram to be considered foreground and Figure 2.17b is the result when choosing both instead. The first cluster contained visually more details from the ECG grid. The second cluster, which is set as foreground in Figure 2.17c, seems to contain darker background colored intensities of the grid. Lastly, the Figure 2.17d can be useful in visual inspection to make an inverted binary of Figure 2.17a by thresholding the intensities that are ≥ 60 to be white.

The threshold examples demonstrated so far are done globally, meaning there is one threshold value to be used for the whole image. There are also local methods where a subset of pixel intensities are observed, and threshold values for each subset is determined. Subsets can be a rectangle shaped slices of the image that do not non-overlap each other, or for each pixel its surrounding pixels are observed with a defined shaped.

The process of finding the optimal threshold value can be automated by using a thresholding method/algorithm. Otsu's method is a global thresholding method,

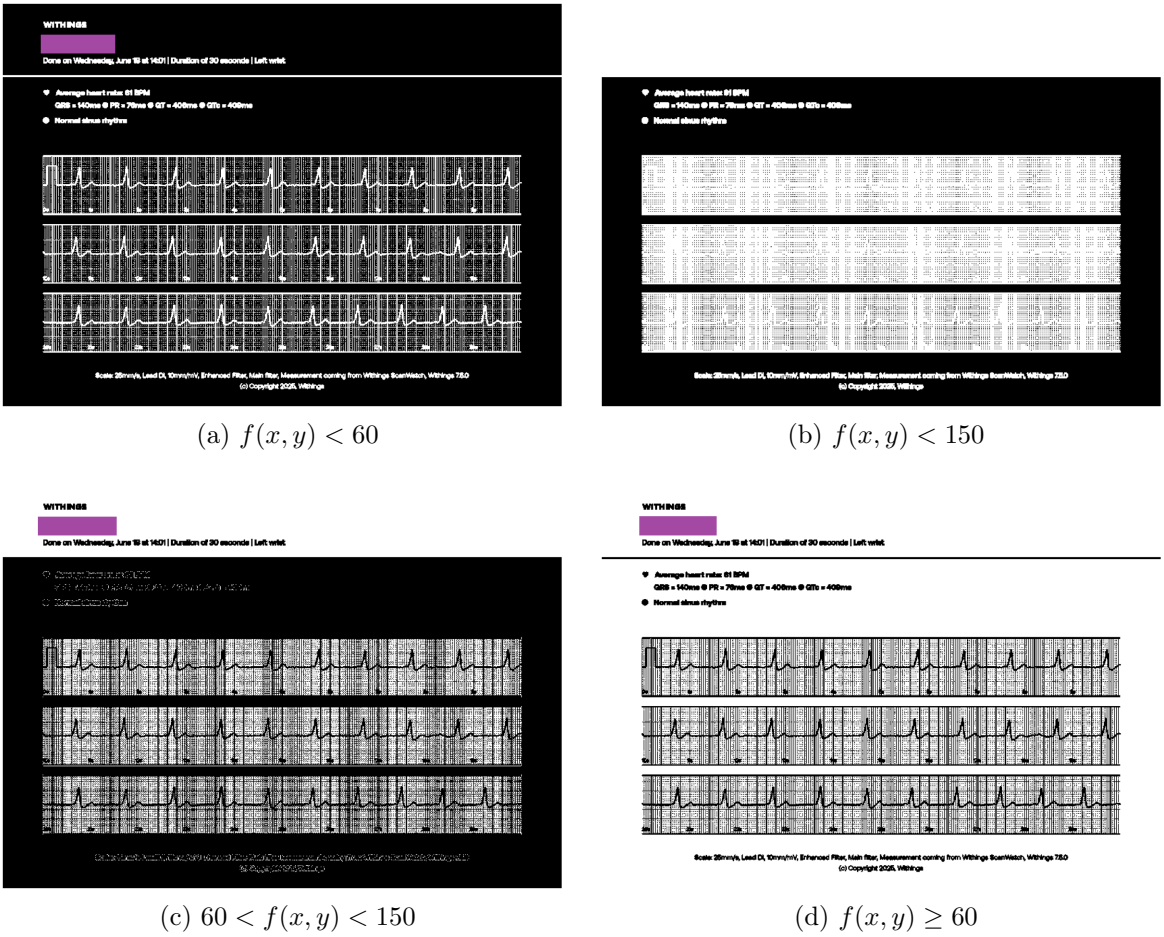

(a) $f(x, y) < 60$ (b) $f(x, y) < 150$

(c) $60 < f(x, y) < 150$ (d) $f(x, y) \geq 60$

Figure 2.17: Thresholding binary images calculated by observing each pixel intensity $f(x, y)$ of the image and determine whether it is fore- or background using one or multiple threshold values.

and is based on finding a threshold that produces maximum variance of the intensity values between the thresholded fore- and background pixels [81]. Skimage python library provides a local thresholding function, that gives a local threshold value for each pixel by calculating the Gaussian mean of intensities in its surrounding pixels (Figure 3.7b) [82].

2.4.5 Morphological operations

The morphological operations are based on one or multiple logic operations to a binary image. These operations are done with a structuring element (SE), which is

also known as footprint and kernel. SE is a binary image with uneven sides, and is probing the image by having its origin (center) go through all pixels in the binary image. The shape of SE refers to the shape of what its foreground pixels are forming. Each pixel in the binary image is evaluated whether the pixel is foreground or background, by using different logic operations to the surrounding pixels that are inside the overlapping SE regions. Dilation and erosion are the fundamental morphological operations which other operations use in varying combinations. Dilation is an inclusive operation, meaning it considers all the overlapping pixels with SE as foreground, if at least one overlapping pixel matches. Erosion is an exclusive operation, meaning that all the overlapped pixels need to match to consider pixel located where SE center is as foreground. Opening operation smoothens the outlines of foreground objects and eliminates objects that are smaller than SE. It is a combination of erosion and dilation by first eroding the image, and then dilating the eroded image. Closing operation closes small gaps in the object that are smaller than SE. Closing does these same operations in different order: first dilating the image, and then opening the dilated image.

Figure 2.18 visualizes these operations with a small, 9×7 sized binary image using a square, 3×3 sized SE of values 1 (Figure 2.18f). The outputs of each operation can be understood by observing what value located in the center SE would be, based on the logic operations explained before for each pixel, and have the results stored in a separate binary image with the same size. On the very edges and corners of the image, the SE is not completely filled with values. This is solved by padding the image edges and corners with zeroes, effectively making the binary image temporarily a 11×9 sized image when the SE is rolling through each pixel.

As explained before, dilation was considering a pixel to be in foreground (1) when any of the pixel overlapping with SE matches. In this Figure 2.18 example the SE

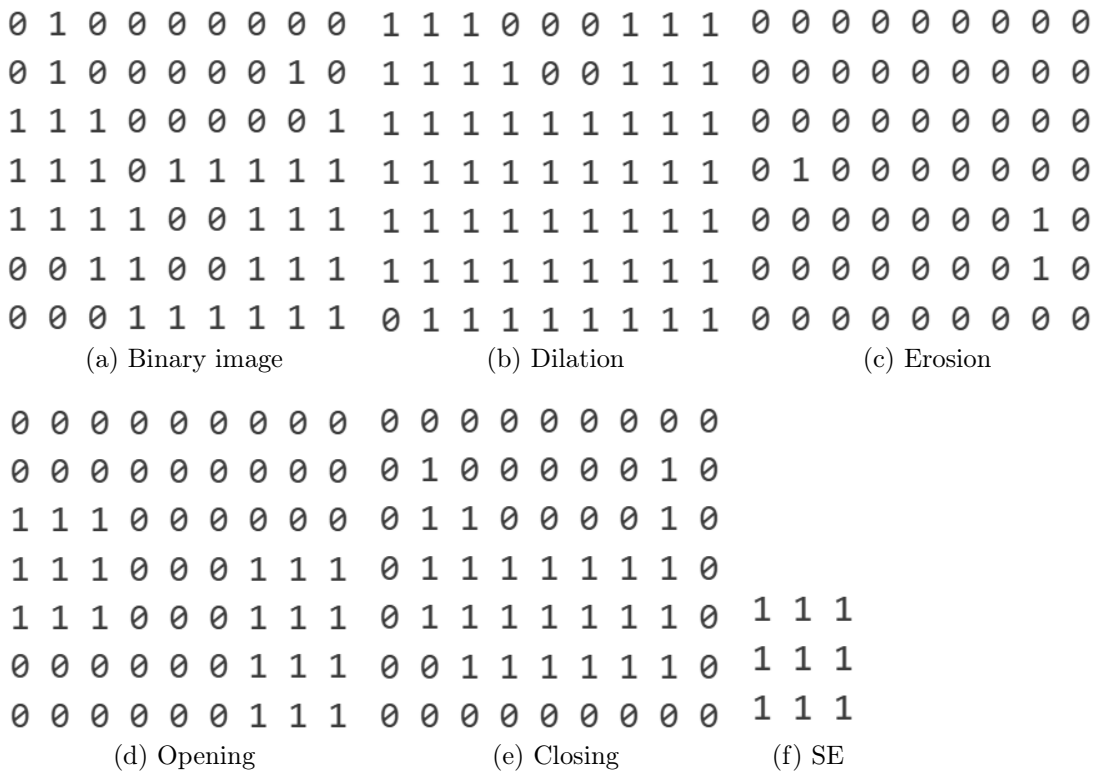

Figure 2.18: Morphological operation examples to the binary image (a) using the same structuring element (f).

is containing only value 1. This means in dilation the pixel is 1, if itself is 1 or any of the surrounding pixel is 1, else it is 0 (Figure 2.18b). For the erosion all pixels had to match, in other words the pixel itself and the surrounding pixels have to be 1 in order to consider it to be 1, otherwise it is 0 (Figure 2.18c). The opening was dilating the eroded image, so the same process can be applied but instead with the erosion result and dilating it. In Figure 2.18d, when comparing opening result with the binary image you can see that it is effectively included only the foreground pixels that completely fitted with the SE, resulting 2 objects where the one on the right fitted SE vertically twice. The closing operation was eroding the dilated image, effectively in the Figure 2.18e example, smoothening the foreground object outlines and closing its small 2×2 gap of zeroes.

3 Implementation

This chapter describes the design and implementation of the AMI detection system named InfarctWatch. It is not designed to have impact for all possible factors towards long patient delay that were discussed in subsection 2.2.1. Patients that identify their discomfort as possible AMI symptoms, but are still hesitant to call emergency medical service are the core target group of this mobile AMI detection service. As seen from Figure 3.1, there are 3 main parts in the architecture: smartwatch provider's system, the patient, and InfarctWatch system. InfarctWatch contains a mobile application named as InfarctWatch app and backend system called InfarctAPI. InfarctWatch app is the interface for the user to send their ECG data they receive from their provider, and also to communicate the prediction InfarctAPI returns. The InfarctWatch app user experience is expected to be same regardless what smartwatch product user owns, as long as the user is able to download their ECG data from the provider system. The overall user experience and AMI detection performance are the most important aspects for InfarctWatch to make a significant impact on reducing the patient delay, and also to provide a seamless, accurate, well communicating mobile AMI detection system for the user.

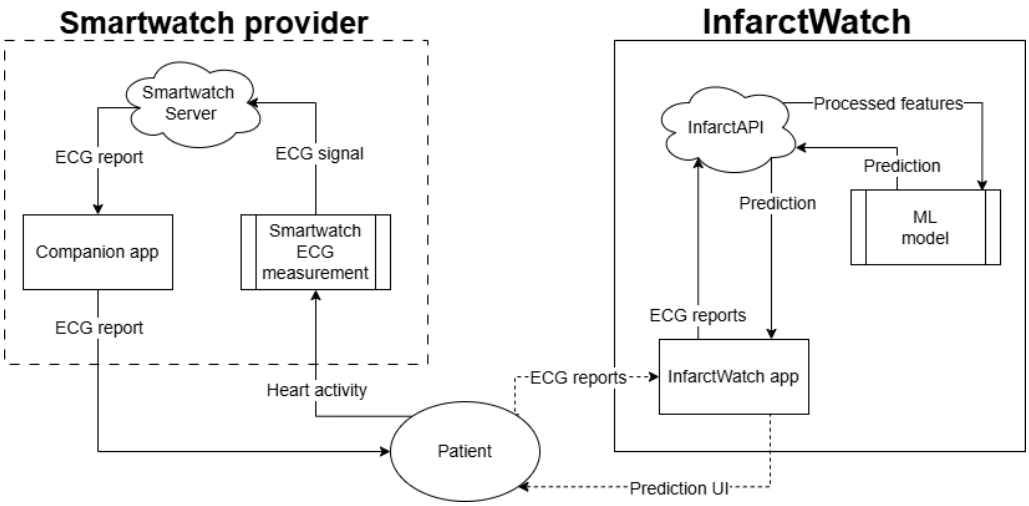

Figure 3.1: InfarctWatch system architecture.

3.1 InfarctWatch app

User is asked to give an ECG file that is measured when they experience no symptoms. This is required to have a healthy baseline data that is used to compare with the data that is measured during suspected AMI symptoms. The healthy baseline is copied to InfarctWatch app directory, and is sent with the input ECG when user is requesting evaluation (Figure 3.4). How InfarctAPI serializes and uses these files to detect AMI is explained in section 3.2.

The most crucial role for the InfarctWatch app is to have a seamless experience for the user to send their ECG data to the app for AMI evaluation. InfarctWatch app is however a standalone application with no technical integration with the smartwatch provider, which has hindered the user experience to send their ECG to InfarctWatch. During the implementation, there were attempts to use the share and "open with" feature that mobile operating systems provide (Figure 3.2). These features feature allows user to open any application that accepts the selected file type, and this application launch action is stored with a link the app could read. This link may lead to the provider's companion app directory, which does not grant read permission to

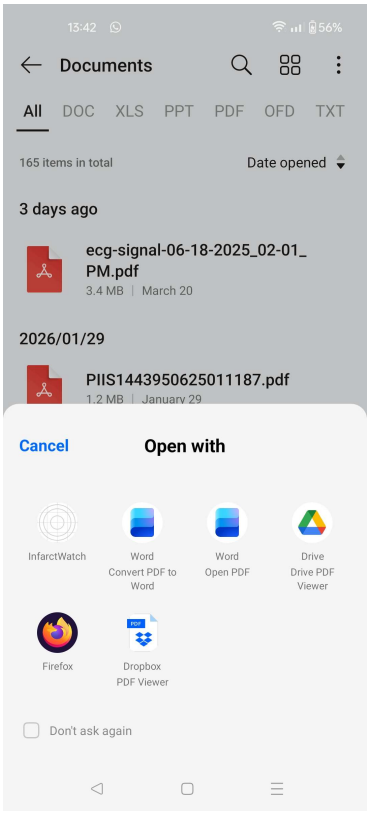

Figure 3.2: Opening the ECG file with the InfarctWatch app.

an unknown application. Because of this the user needs to download it to their file system, which grants read permission for any app. There was also an experimentation with Bluetooth Low Energy (BLE) connection capabilities whether it could give access to the ECG data when user measuring the ECG with the smartwatch. The experimentation did not however find a way to even connect the InfarctWatch app to the Withings device, even when it was connected to the device for the Withings companion app. How the user can give their ECG to the InfarctWatch app was in the end simplified by instructing the user to only select the file by pressing a button inside the app.

Once the file is downloaded to the read grant giving folder, user can open the InfarctWatch app, press the select file button, and find the downloaded file from the file system. If user was in selecting their healthy baseline file, the file is copied to

InfarctWatch app directory for later use. If user wanted the file to be evaluated for AMI, then the selected file and the stored healthy baseline file are Base64 encoded and sent in a POST API request payload to the InfarctAPI. The InfarctWatch app expects the API request to respond with value 0, when InfarctAPI did not detect AMI. When AMI was detected, the API is expected to return value 1. If the request failed an HTTP error code is assumed. On infarction case the user is instructed to call an emergency number with a button that opens a deeplink. This takes user to the phone's dial number view which has the emergency number prefilled. In a case when AMI was not detected, it does not necessarily mean user did not experience AMI. The app tells this, and advises the user to read the help page, which contains information about AMI symptoms. The help page is accessible at any time in the app. It lists common and some less common AMI symptoms, and instructs the user to call emergency number if experiencing any listed or unlisted symptoms. To summarize, the InfarctWatch app consists of 3 main functions: set a healthy baseline ECG, find infarction from an ECG, and providing an info page of AMI symptoms to encourage and educate the user to call to the emergency number early.

There are 2 paths to set the baseline healthy ECG: when asked on first time opening the app (Figure 3.3a), or update it in the home screen (Figure 3.3b). The help page lists the AMI symptoms including a short description. All the symptom descriptions are visible by default, unlike in Figure 3.3c, where some of them are toggled hidden by pressing the bolded symptom for demonstration purposes. The ECG evaluation starts (Figure 3.3d) by pressing the first button in home screen. The evaluation ends when the app shows the prediction response (Figure 3.3e or Figure 3.3f).

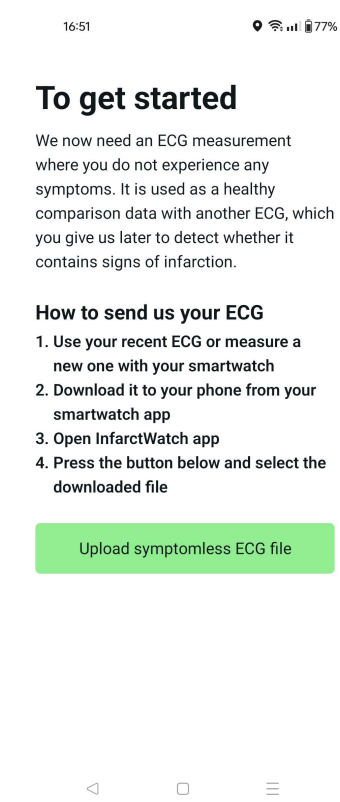

(a) First time opening the app

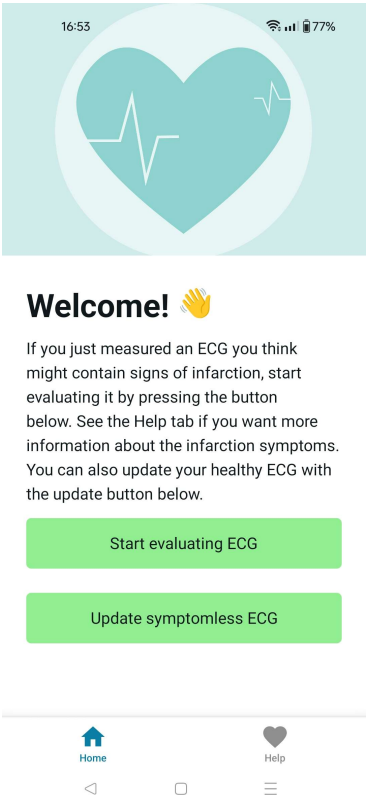

(b) Home screen

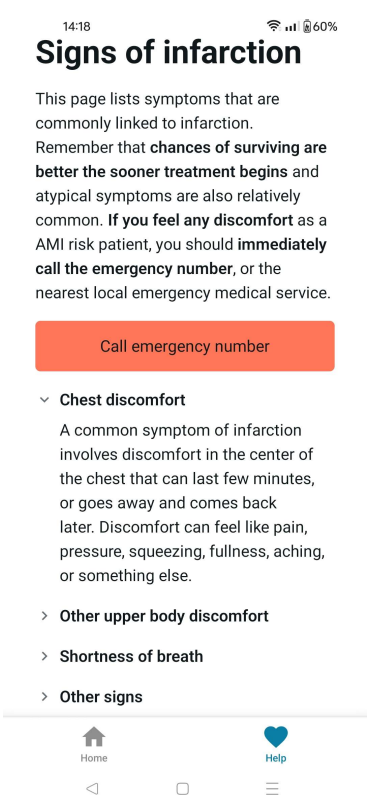

(c) Help page

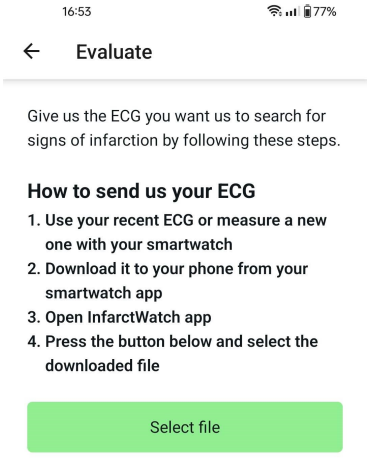

(d) Start of the ECG evaluation

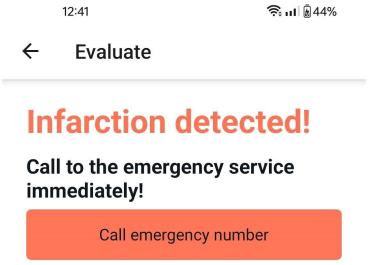

(e) Infarction predicted

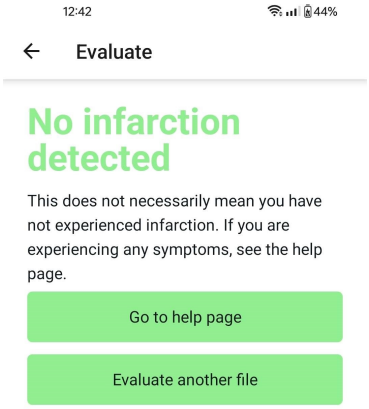

(f) No infarction predicted

Figure 3.3: InfarctWatch app views: (a) home, (b) help, (c) start of evaluation, (d) infarction predicted and (e) no infarction predicted.

3.2 InfarctAPI

InfarctAPI prediction endpoint expects the request payload to contain a healthy baseline ECG report and the input ECG report. The ECG signal from both of these PDF formatted reports are extracted, their signal is preprocessed and features calculated. The difference of these features are given as an input to the machine learning model, which prediction is then returned to the InfarctWatch app as API request response. In other words, InfarctAPI has 4 core processes: ECG signal extraction, signal preprocessing, feature calculation, and ML prediction (Figure 3.4).

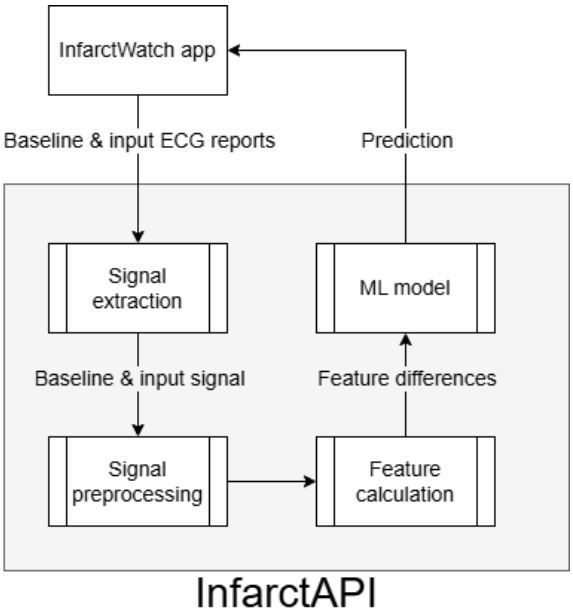

Figure 3.4: Data flow and processing logic within InfarctAPI.

3.2.1 Smartwatch ECG report

ECG report that is generated from the smartwatch ECG signal differs between providers. User is able to access the generated ECG report with a companion app made by the producer that user needs to install into their smartphone. Somehow the ECG needs to be extracted and digitized from the PDF formatted report. For context, the annual George B. Moody PhysioNet Challenge contest invited teams to

solve similar extraction problem [83]. InfarctWatch implementation however, uses an open-source ECG-digitizing algorithm developed by Fortune, Coppa, Haq, *et al.* [84] to solve this core piece of the puzzle. They had developed and validated their algorithm by using clinical ECG data which contained in both paper and digital format. Along with this algorithm, they also made an application with graphical user interface (GUI), where a scanned ECG paper image (Figure 3.5) can be preprocessed by human. Rotating the scanned image, selecting lead locations, set lead start time, and grid scales are the operations the application provides to the user. ECG-digitizing algorithm crops the preprocessed image based on the given lead location configuration before the serialization starts.

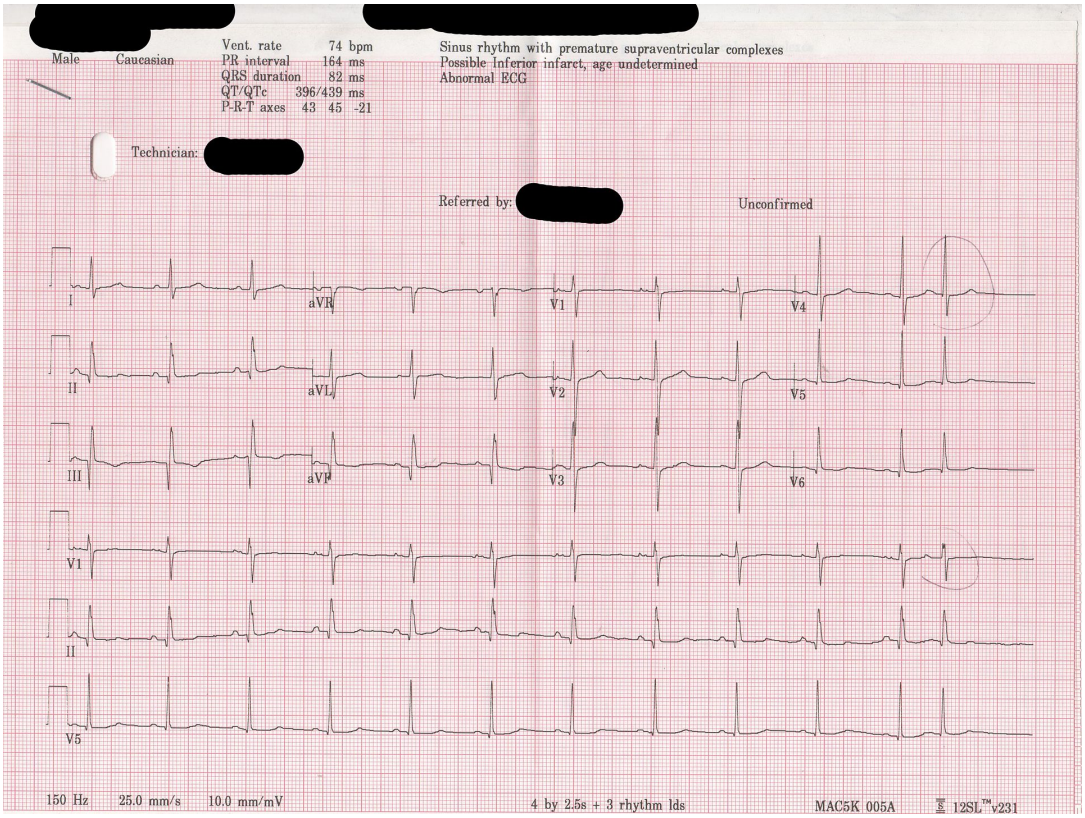

Figure 3.5: Printed ECG paper example containing multiple lead data [85].

The GUI application is not applicable for InfarctAPI, because that part of the process needs to be automatized. InfarctAPI therefore needs its own algorithm to find the lead regions in the image to pass it as a parameter to ECG-digitizing

algorithm. Compared to paper ECG the smartwatch ECG report also contains only one lead, and the rotation is expected to be fixed. Smartwatch ECG reports may differ between different providers in image resolution, smartwatch sampling rate, and the grid scaling (mm/s horizontally and mm/mV vertically). To simplify the first version of InfarctAPI, the time and voltage scaling parameters are always given as 10 mm/s and 25 mm/mV respectively. Withings and Huawei smartwatches, that were used during implementation, had these scaling values in their reports (Figure 3.6).

Figure 3.6: Cropped ECG report from Withings Scanwatch.

The ECG signal is extracted from this PDF formatted report by first converting it to an image. After conversion, various image processing techniques (section 2.4) are utilized. The image resembles an A4 paper page with some content positioned on the top, leaving in some reports a lot of empty space underneath the content. To improve processing time, the image size is reduced by cropping out the empty space with a small safety margin. This content area is determined by first greyscaling the image,

and then making a binary image with Otsu's threshold method (subsection 2.4.4). The rectangle shaped bounding region of the foreground is determined by finding the minimum and maximum pixel coordinates in x and y axis containing value 1.

Once image is cropped based on the detected foreground region, the image is once again greyscaled and made into binary image, but this time for finding the grid regions. To detect subtle contrast that some ECG reports may have, the histogram of the greyscaled image is equalized (3.7a) before thresholding. Local thresholding is used to make sure fine grid area details remain in the binary (3.7b). If grid color is almost the same as the background, but other content is in high contrast, then non-local thresholding methods would have too high threshold value. This would result the grid area considered as background (valued 0) in the binary image. Next, the grid area needs to be somehow highlighted. To achieve this, the small gaps the grid area has are closed, ideally turning the grid areas into large, distinct rectangles like in figure 3.7c. To filter out the other objects, opening method is used with a large rectangle structuring element (3.7d). Opening and closing methods are explained in subsection 2.4.5.

Now that the regions are found, the inputs for ECG-digitizing algorithm are ready. The signals that are extracted from each region are appended into one raw signal. Figure 3.8 shows a short segment of the ECG extracted from the Withings ECG report. Appendix B shows the same digitizing process of an ECG report from Huawei smartwatch. Signal from Withings contains poor morphological details due to the low resolution of the image. The total signal length for the 30-second period was 2065 from Withings and 9428 from Huawei report. When the signal length is divided with 30 seconds, the extracted signal "sampling frequency" can be calculated, resulting 68 Hz and 314 Hz for Withings and Huawei respectively. This demonstrates how the report resolution is an important factor for signal quality.

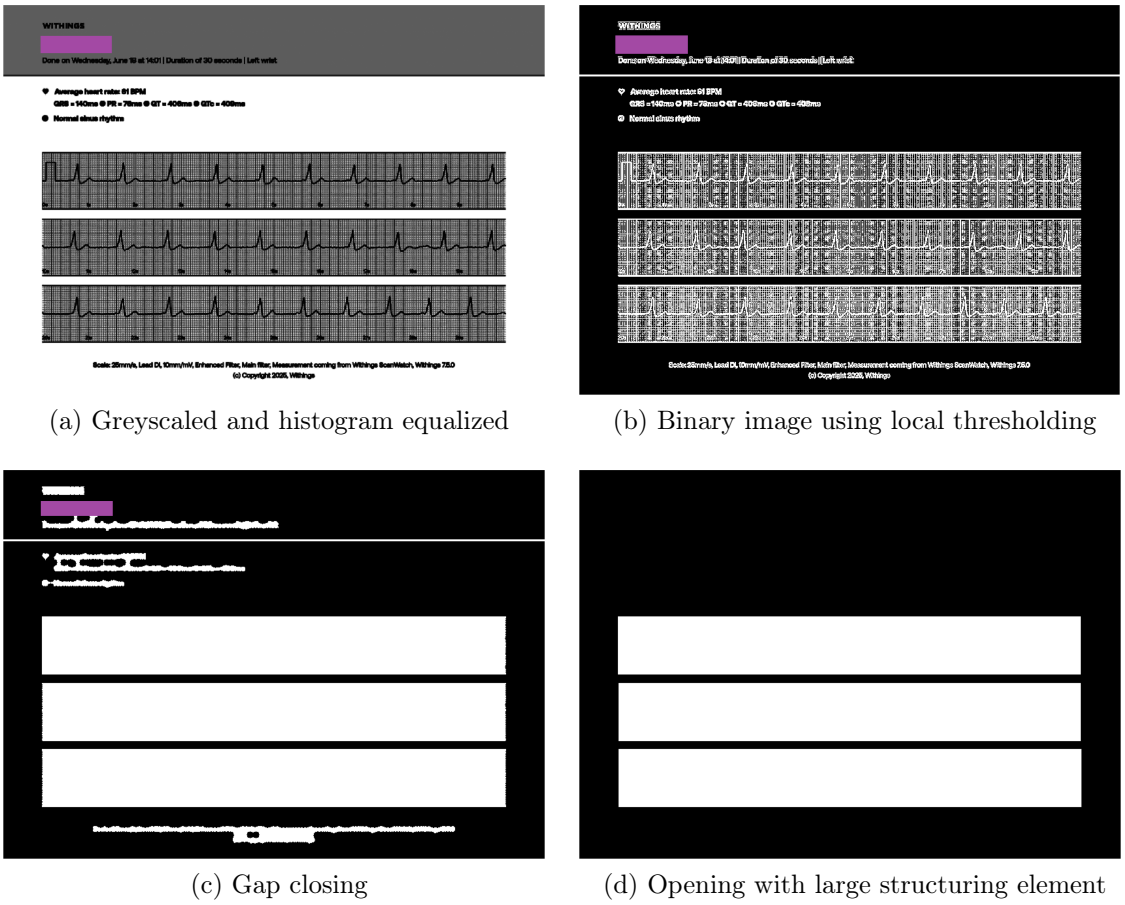

(a) Greyscaled and histogram equalized

(b) Binary image using local thresholding

(c) Gap closing

(d) Opening with large structuring element

Figure 3.7: Cropped Withings ECG report processed by grid detection algorithm.

The sampling frequency of the smartwatch ECG sensor becomes less relevant since the source of the signal is instead from an image drawn by the smartwatch provider.

Before the signal is filtered the first half second of the signal is removed to make sure the possible calibration mark is not included in the signal. ECG paper commonly has this rectangle shaped calibration mark at the beginning to indicate the height of 1 mV amplitude and width of 0.2 seconds [86]. The signal is filtered with windowed median filter to remove the temporal detection errors by the ECG-digitizing algorithm, and then smoothened with a moving average. Filtered signal is now ready to be further preprocessed for the ML model prediction. The preprocessing step and the feature calculation (Figure 3.4) is the same for the data that is used for the model training, which is why they are explained in subsection 3.2.2.

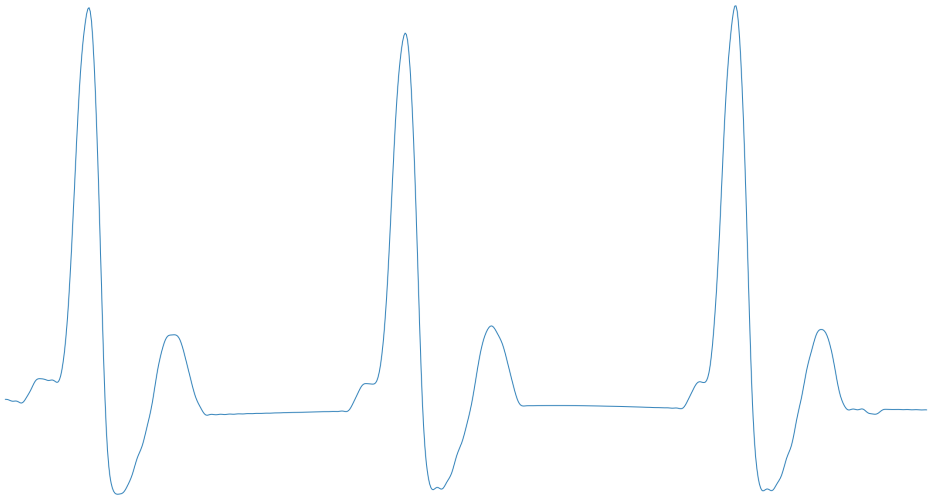

Figure 3.8: A segment of preprocessed ECG signal.

3.2.2 Machine learning model

Total of 97 patient data were included from the STAFF III database (subsection 2.2.2) to the model dataset. There were 71 patients who had their ECG measured twice before the inflation procedure. The data points for model training and testing (section 2.3) are the feature differences between either two healthy ECGs, or ECG during inflation and the latest pre-inflation ECG. In other words, model dataset contains 71 healthy and 97 infarction data points for training and testing. The ECG signals needs to be first preprocessed, biomarkers detected, and features calculated in order to make these data points.

Preprocessing

In preprocessing, the signal sampling rate is made static value of 250 Hz by resampling the signal first, which also reduces overall computation time. The signal is then filtered with 2 filters. First is a bandpass filter with cut-off frequencies of 0.5 and 40 Hz to remove noise. Second is a moving average filter with window size of 5 to smooth out the short-term fluctuations from the signal.

Biomarker detection

ECG peaks and segments (Figure 2.6) need to be detected from the signal first before extracting metrics. There are libraries that provide functions to detect the ECG peaks and some wave offsets and onsets. There were no methods available for finding S wave offset and Q wave onsets, which is why custom segment detection algorithms were implemented. Finding biomarkers usually starts by finding the R peaks in the signal and its locations are used to find other peaks. This can be achieved by enhancing this highest peak in the heart cycle with same steps as in Pan-Tompkins algorithm. This algorithm consists of bandpass filtering the signal (which is already done in preprocessing), calculating the temporal signal changes with the derivative of the signal, square the derivative so that the steeper changes are more visible, and finally do a small windowed moving average to get rid of other high peaks (Figure 3.9) [87].

Scipy library provides a function to find the prominent peaks from the input signal [88]. Minimum distance between peaks and minimum height of the peaks were given as a parameter to make sure correct peaks are detected. Minimum distance is effectively the minimum time between peaks in time series data. This parameter was set to allow 4 beats within a second, which corresponds to impossible maximum heart rate of 240 bpm, and is simply calculated by dividing the static sampling frequency by four. The minimum height was calculated using the mean value of the peak enhanced signal, and multiplying this mean value with 1.5. The peak enhanced signal was given as the input signal to the scipy's function that returned the time indices of the R peaks, which were used to find the real R peak location in the signal segment (Figure 3.10).

Now that the R peaks are found, other peaks can be found by first calculating a peak searching windows where a peak should approximately locate. Precise location is

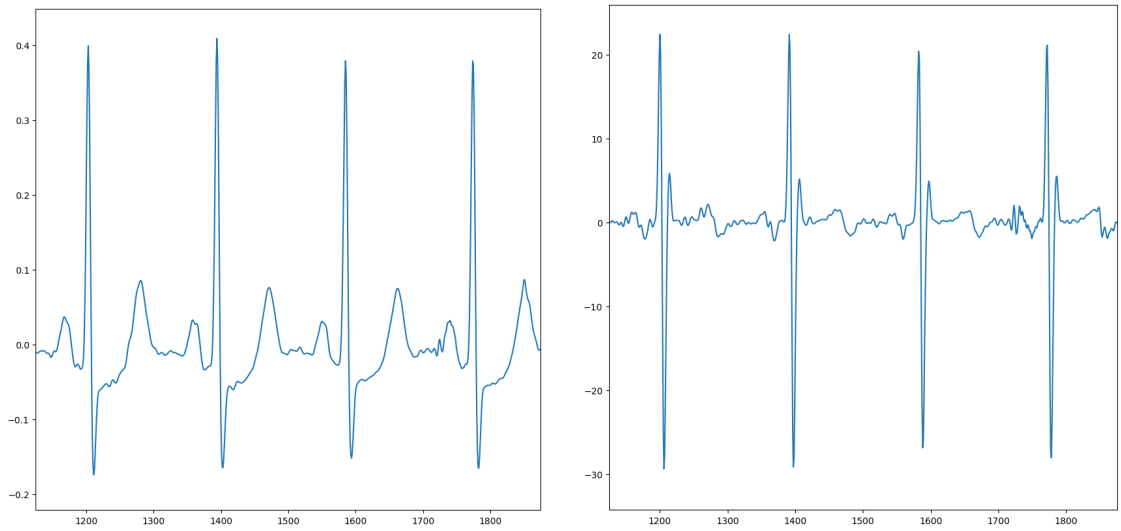

(a) ECG segment

(b) Signal derivative

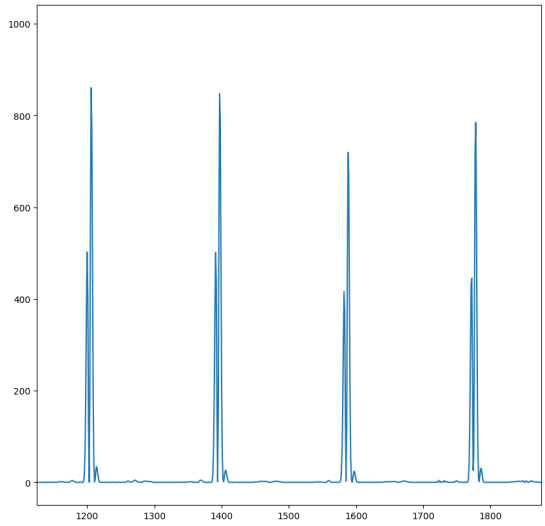

(c) Derivative squared

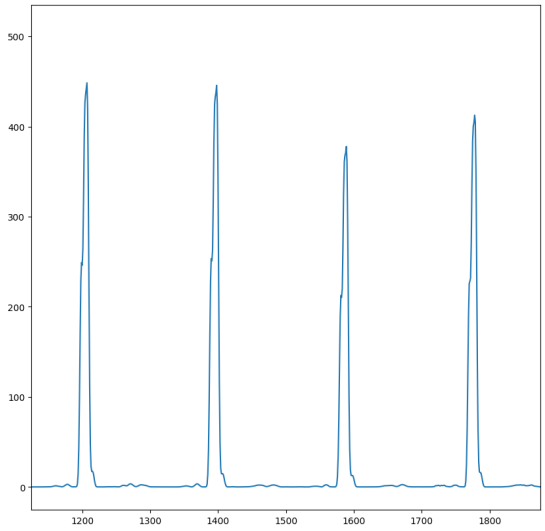

(d) Averaged

Figure 3.9: Process of making R-peaks more prominent for peak detection.

found by observing the signal values inside this window with different mathematical operations. The mean RR interval (MRRI) is also used to determine the window location and width. Given the fact that record duration ranges between 1 min 30 s to 9 min 52 s [73], the signal is first segmented to a list of 30 second segments to make sure signals that have high RR interval variability will get more localized mean estimation. The smartwatch ECG that the API will receive is only 30 seconds long, which is why only 10 second segments are used when calculating ECG features

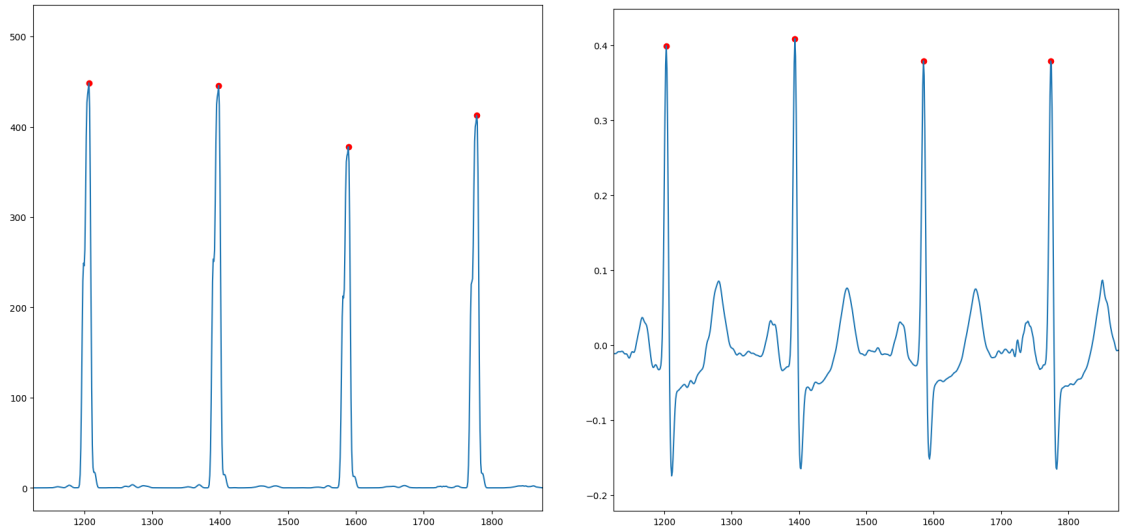

(a) R peak time indices detected from enhanced signal

(b) The real R peak locations in segment

Figure 3.10: R-peak locations in the segment using detected time indices.

during the API request.

The MRRI is treated as an approximated length of one heart cycle, where the R peak occurs at the half-length. For P peak, the center of the search window is calculated by extracting 20% of the MRRI (0.2 MRRI) from the R-peak and the window width is also 0.2 MRRI. Within this search window, the maximum signal value is used to find the P peak location (Figure 3.11a). Q and S peaks were found by making a 0.15 MRRI wide window, centered at the R peak and the minimum values were read from both sides of the R peak (Figure 3.11b). T peak search window was centered in 0.33 MRRI after R peak occurrence with a width of 0.3 MRRI (Figure 3.11c).

Now that all the peaks are found the PQ- and ST-segments (Figure 2.6) are the remaining biomarkers that need to be detected before feature calculation. The PQ segment is supposed to start where the P wave ends (offset) and where the Q wave starts (onset). ST segment starts where the S wave ends (also called as J-point) and where the T wave starts. The previously mentioned wave offsets and onsets need to be somehow found. This is achieved by using the peak locations as the searching

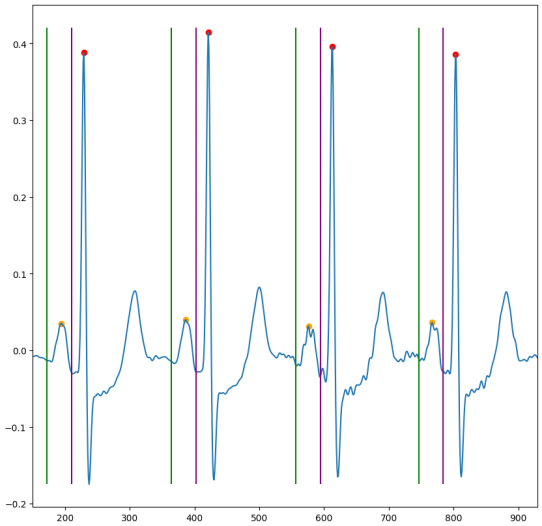

(a) P-peaks

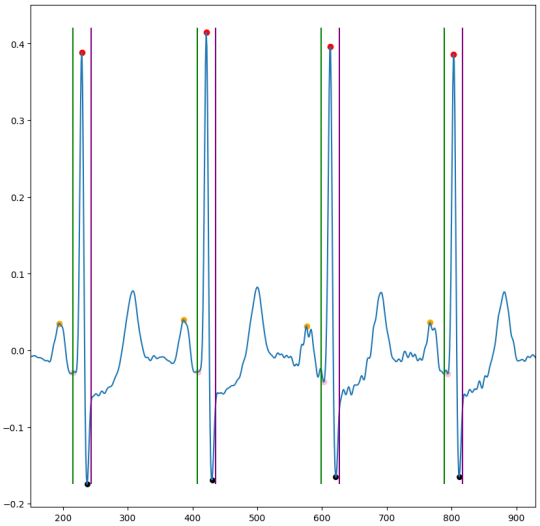

(b) Q- and S-peaks

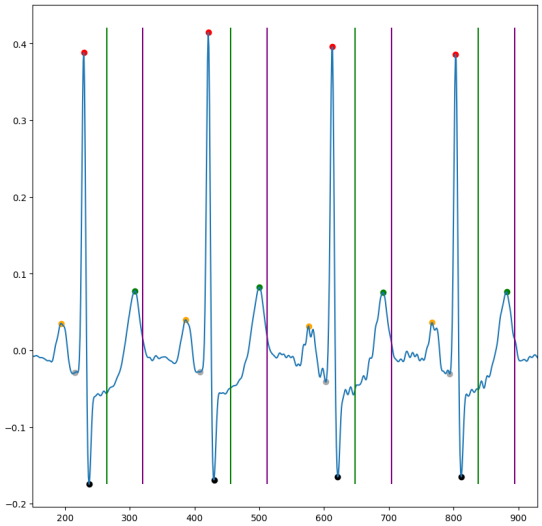

(c) T-peaks

Figure 3.11: Windowing methods to find peaks.

window once again, but this time multiple methods have been developed. These methods are used in order until one of them returns a result. For the both segment search windows, a small margin is included since the waves should not start or end too soon after peak.

For the PQ segment searching algorithm, the first method to find the P wave offset and Q wave onset is a derivative method, where the direction of the signal is an-

alyzed. First this small window segment is preprocessed with a moving average to filter out possible remaining noise induced oscillation in the signal. After this, the unsharp masking procedure is done to highlight the direction changes in the signal. This is a common procedure in digital image processing (subsection 2.4.1), but is also applicable in signal processing. The first derivative is taken from this preprocessed segment. From this the values that are below zero, meaning when the signal going downward are collected. When visually inspecting an ECG signal, even at the point where signal clearly is only going downwards there may be short time periods, where the signal remains the same or goes up. To make sure these small direction shifts in the signal are not found relevant the neighbor values are also required to go downwards. This means that three consecutive derivative values need to be below zero in order to be considered to be relevant. This downward direction observation is used for detecting P offset point, where the P wave downward direction stops at the start of the window. For Q wave onset the signal goes downward again after the P offset, but a small period is required to pass before any downward direction is considered. If the derivative method described above does not yield a result, then a min max method is used. This is essentially finding a location of minimum signal value for P wave offset point near the start of the search window. For the Q wave onset, the location of maximum value near the end of the search window is searched. If this method does not return any results the offset and onset defaults to the edges of the margined search window.

ST segment searching algorithm uses similar methods but also includes one more method that is used before min-max searching. For the derivative method positive values are observed instead of negative. This means now the upward change of the signal is used and not downward. Also, the derivative needs to have five (instead of three) consecutive positive values before it is considered relevant. When the upward direction ends the first time it is considered to be where the S wave offset

locates. The next method is observing zero crossings of the signal, in other words observing when signal direction changes from upwards to downwards, or vice versa. The window is unsharp masked the same way as in the derivative method and then the 2nd derivative is calculated. The first zero crossing is taken as S wave offset and then, by first ignoring a small period of time, another zero crossing is selected as T wave onset. If zero crossing does not return a result, the next method searches the maximum value from the start of the window to determine location of the S wave offset. For T wave onset the minimum value at the end of the window is searched. This algorithm does not default back to any values and therefore may not return any result.

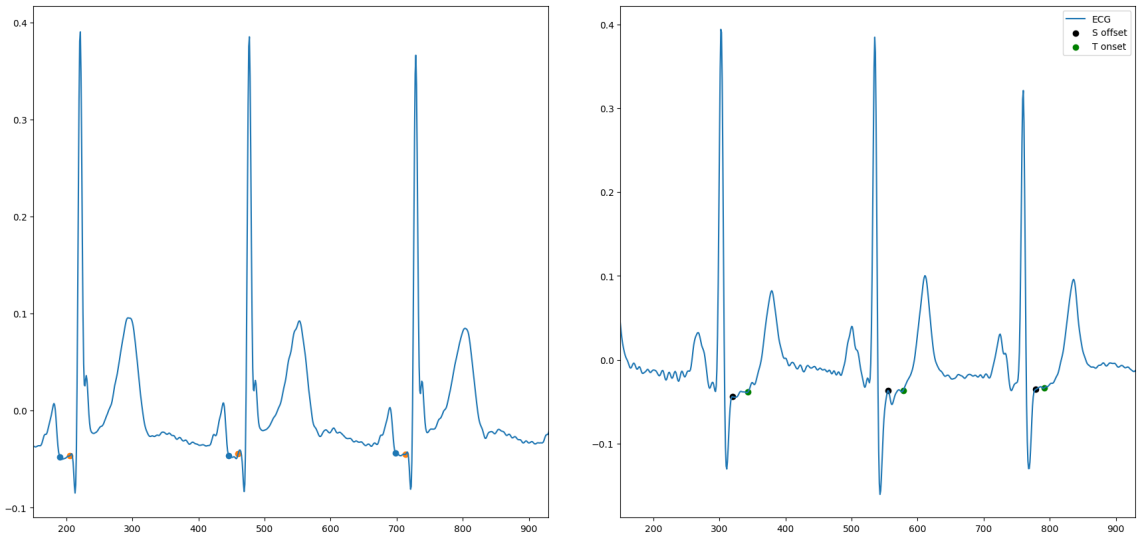

(a) PQ-segment (b) ST-segment

Figure 3.12: Example results from the segment detection algorithms

As seen from Figure 3.12, the algorithms are not giving very accurate results with a signal that contains noise even after preprocessing it. These biomarker results from algorithms were compared with QT-database [89], which contain manually annotated ECG data for the peaks and the onsets and offsets of waves. This comparison simply was done with a visual inspection (Figure 3.13). No deeper statistical analysis were made between the annotation locations in the signal and the results from

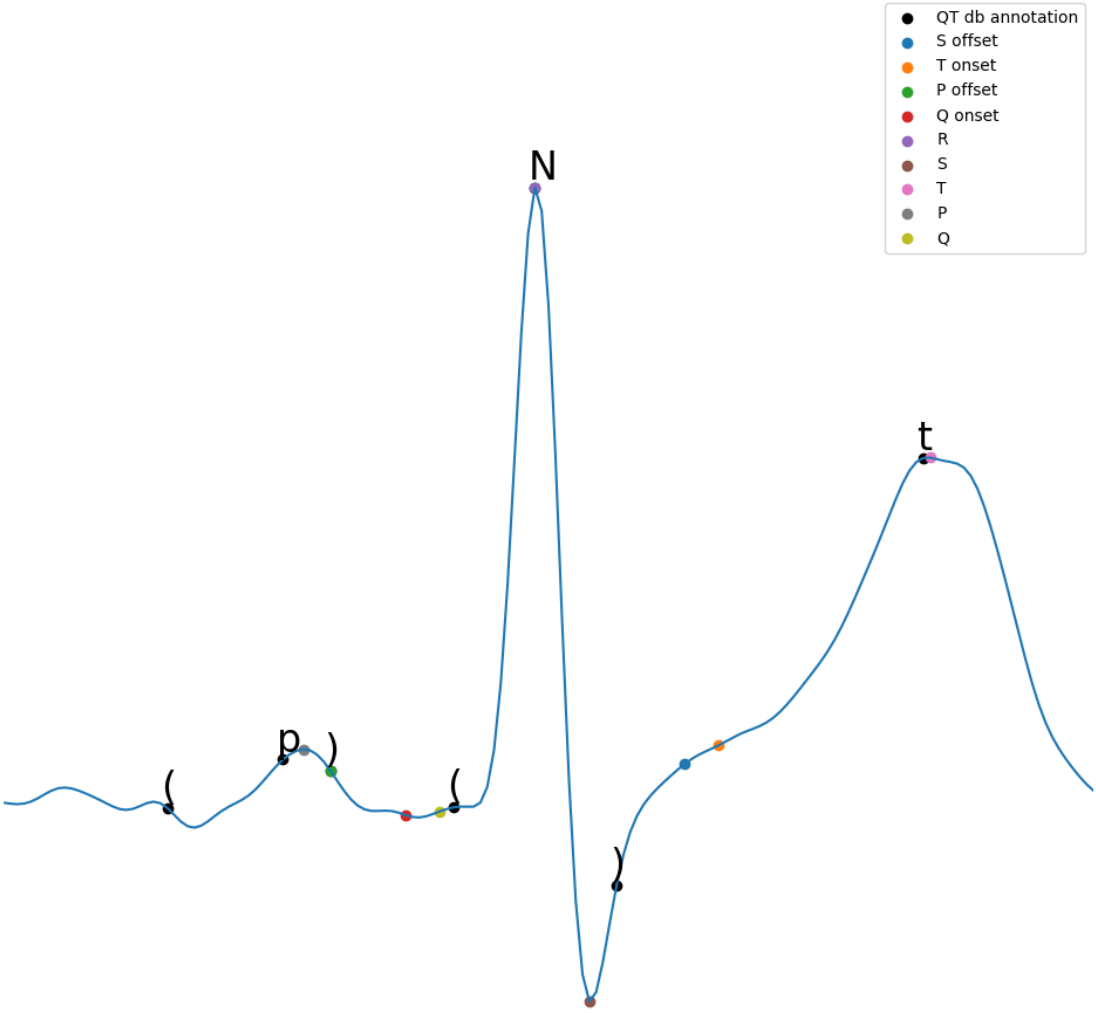

Figure 3.13: Annotation comparison between QT database signal and implemented algorithms. The text annotations and parenthesis are the QT database annotations. Black parenthesis indicates the onset and offset of a wave that is annotated with a respective letter.

implemented algorithms.

Feature calculation

Features from the preprocessed signal are extracted using different kinds of metrics from the whole signal, and from metric changes between segmentations. The feature extraction and selection for the InfarctAPI model was at first following the approach of Sandelin [9], excluding HF-ECG related features. Feature modifications, additions and exclusions were later done to improve model performance. Power, entropy, dominant frequency, and skewness were calculated in signal's frequency spectrum. Kurtosis was calculated in the wavelet spectrum. Each segment had their biomarkers detected first (section 3.2.2). Out of all the detected R peaks in segments the root mean square of successive differences (RMSSD), standard deviation of RR intervals (SDRR) and the mean peak amplitude were calculated. Some signals had no other detectable peaks around the R peak. ST and PQ segment lengths and amplitudes were therefore calculated only from heart cycles with all peaks detected.

The mean waveform of the segment was calculated to determine slope and T-wave angle of the total mean waveform across all segments. In order to calculate the total mean waveform, the waveforms per segment were first resampled to same length (Figure 3.14). The slope of total mean waveform was found with TSFEL (Time Series Feature Extraction) library. Their method returns the m coefficient of linear equation $y = mx + b$ which is fitted over given signal amplitude values (Figure 3.15a) [90]. T-wave angle is determined by first finding the steepest upward $\mathcal{I}_1$ and downward $\mathcal{I}_2$ slopes of the wave. With these slopes, their respective lines are drawn and the angle ϕ, which is formed by intersection of the lines, (Figure 3.15b) is calculated using euclidean based Equation 3.1. This kind of approach Lázaro, Alcaine, Romero, *et al.* [91] also utilized in their QRS study for measuring R wave angles.

$$\phi = \arctan\left(\frac{\mathcal{I}_1 - \mathcal{I}_2}{1 + \mathcal{I}_1\mathcal{I}_2}\right) \tag{3.1}$$

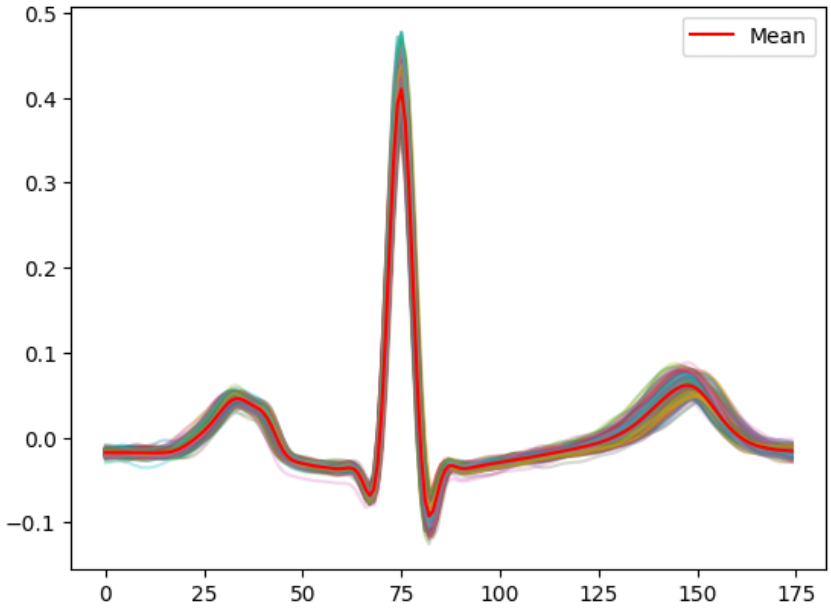

Figure 3.14: Mean (resampled) waveforms per segment and their total mean waveform from an ECG signal that is recorded in resting room.

Modeling

Once features are extracted from all recordings, the feature differences between the two pre inflation, or the inflation and one pre inflation is calculated. These differences are then labeled to healthy and infarction binary classes $\{-1, 1\}$ respectively. Feature differences that contained recordings during the balloon inflation procedure were labeled to infarction class (1), and differences with only pre inflation recordings to healthy (-1). Appendix C shows all the feature differences in the dataset with box plots, showing the outliers and spread of the values in quartiles. The dataset is then split for model training and testing. Training split contains 80% of the dataset and test the remaining 20%. The data points were assigned to the splits randomly. To make sure one of the splits contain enough data points for both labels, the stratification is used. It makes both splits have near equal ratio of both

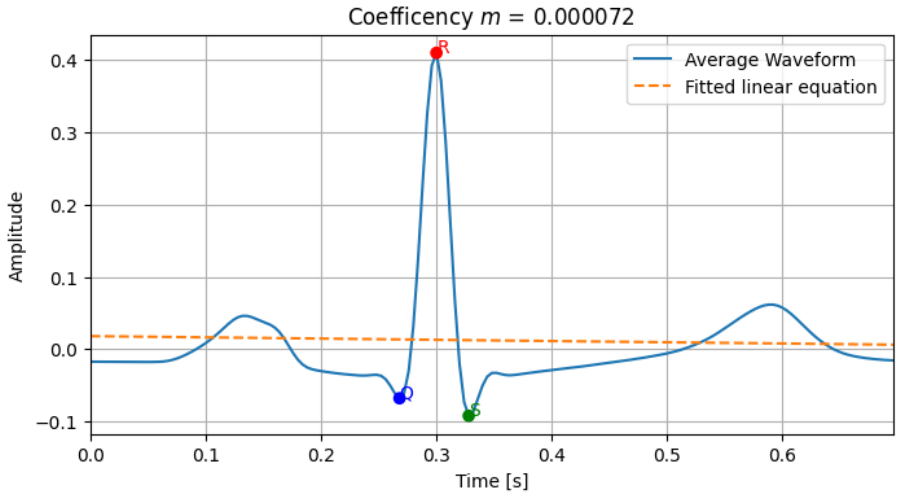

(a) Slope of the average waveform.

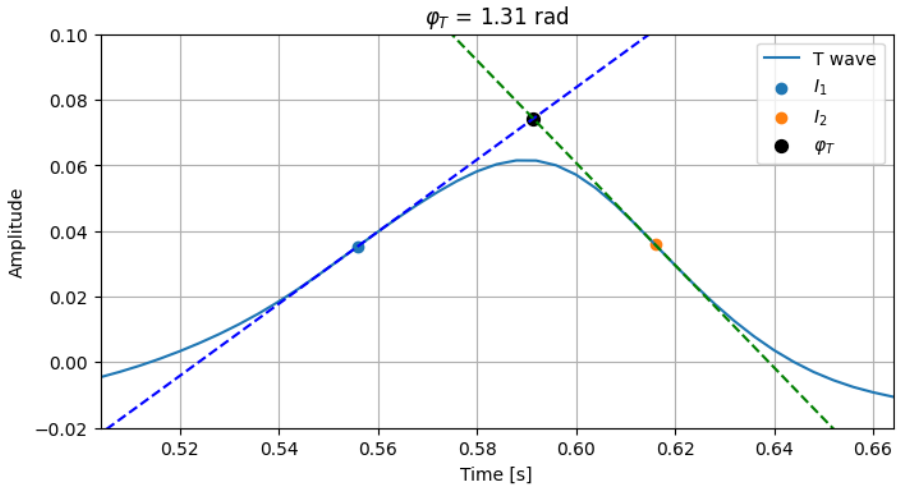

(b) T-wave angle calculation

labeled data points. The training split contained 55 healthy and 77 infarction labeled data points, and the test split contained 14 healthy and 20 infarction labeled data points. There was no grouping done during the data split, meaning the same patient's healthy and infarction labeled data point may be in different splits. This was not seen as a necessary procedure, because the model is trained by observing feature differences between different ECG recording sessions. This should not make temporal or patient based bias to the model prediction.

The training data points are normalized with a RobustScaler provided by the Sklearn

library [92]. RobustScaler normalizes each feature by subtracting its mean and scales the values to be between -1 and 1 based on its interquartile range. By doing this the normalization process is not affected by few large outliers. This was seen as an advantage for the real use case where patient signals may have significant outliers due to possible noise from motion. The median and IQR of each feature in the training set is stored in order to normalize the test split. Since the data points are normalized for the model, the ECGs that the patient sends through InfarctWatch app also needs to be normalized with the same median and IQR. This ensures that in testing and in real world use the data points are normalized with the same statistical properties with training split.

Random forests, decision tree, extra tree and K nearest neighbor classifiers were used for finding the best predicting model. Leave-one-out (LOO) cross-validation (CV) process was used to get prediction performance metrics from each classifier. This process iteratively trains a new model with the same classifier using a subset of the training set. LOOCV leaves one data point out from the training set and uses it to test the trained model whether it can predict the label value. This effectively means that the classifier performance is cross validated as many times there are data points in training split, where each data point is tested using remaining data points, and each prediction result is stored. Random forest classifier method showed the most promising prediction metrics from its LOOCV results. Its results with test split is discussed in chapter 4.

4 Results

When testing the trained random forest model with the test split, the confusion matrix gave suboptimal results in classifying healthy data points (Figure 4.1a). Figure 4.1b shows the receiver operating characteristic (ROC) curve of the prediction performance with test data. The high area under the curve (AUC) value of 0.96, and when inspecting the curve indicates that tuning the model decision threshold value to be a promising next step to improve its performance. Decision threshold is the minimum confidence value the binary classifier would classify the data point to be labeled 1 and otherwise -1. When this threshold is tuned, it will mean in this case that there will be more true negative classifications with the expense of increasing the false positive classification rate. The tuning needs to have a scoring metric to optimize towards. To make sure prediction performance for both labels are near equal, the balanced accuracy scoring was used. This scoring method calculates in binary classification the mean of true positive rate and true negative rate (Equation 4.1) [93]. The best score of 0.815 was received with a 0.643 decision threshold (Figure 4.2b). As seen from Figure 4.2a the results improved considerably, with only 3 total misclassifications out of 34. From this final tuned model, the test split resulted 0.912 accuracy, 0.947 precision, 0.9 recall and 0.923 F1-score.

$$\text{balanced accuracy} = \frac{1}{2}\left(\frac{TP}{TP+FN} + \frac{TN}{TN+FP}\right) \tag{4.1}$$

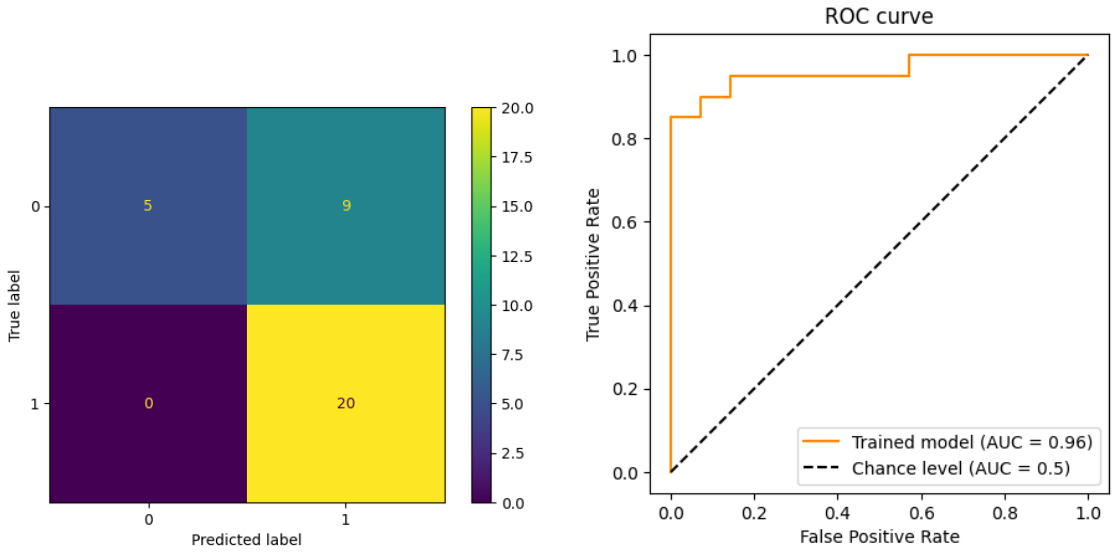

(a) Confusion matrix (b) ROC curve

Figure 4.1: Random forest model results with test split data

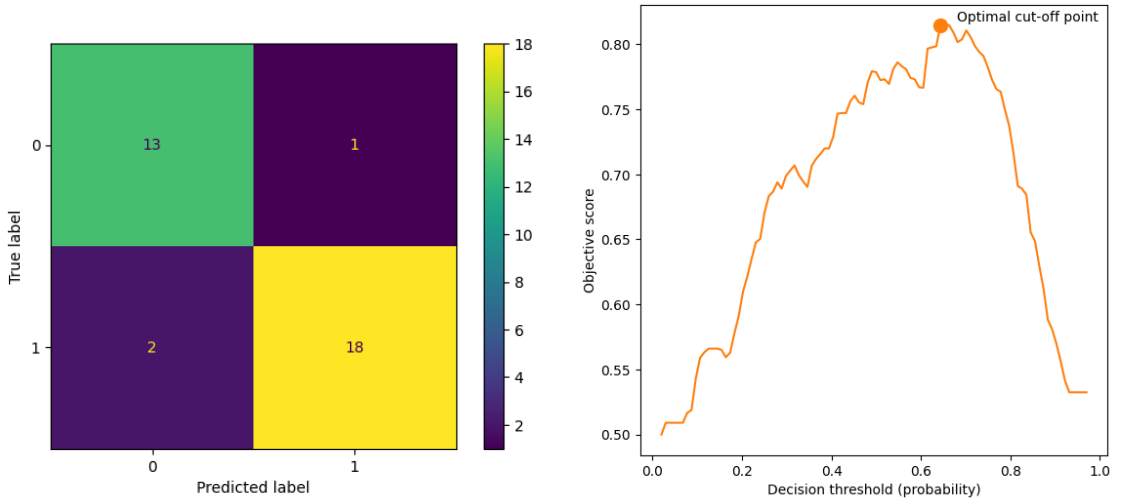

(a) Confusion matrix (b) Score results with different decision thresholds

Figure 4.2: Decision threshold tuned model results

The model prediction metrics with a test split does not mean model was able to find a hypothesis that generalizes to unknown data. Especially with input ECG signal that is extracted from an image and measured by a patient using a commercial smartwatch, as opposed to a medical grade ECG signal measured by a professional. The InfarctWatch AMI detection capabilities were tested with four different smartwatch models and 12 subjects. Withings ScanWatch was tested on nine subjects,

Age	FP (n)	TN (n)	Smartwatch model
11	0	1	Withings ScanWatch
15	2	2	Withings ScanWatch
21	0	1	Samsung Galaxy Watch 4
33	6	1	Withings ScanWatch
33	0	1	Withings ScanWatch
33	0	1	Polar Vantage M3
34	1	0	Withings ScanWatch
34	0	1	Polar Vantage M3
49	1	0	Samsung Galaxy Watch 4
53	0	1	Withings ScanWatch
57	2	1	Huawei Watch Ultimate
60	0	1	Huawei Watch Ultimate
60	3	0	Withings ScanWatch
74	0	1	Withings ScanWatch
76	0	1	Withings ScanWatch

Table 4.1: InfarctWatch infarct detection test results with commercial smartwatches. TN = True Negative = Infarction not found; FP = False Positive = Infarction found;
.

Huawei Watch Ultimate on two subjects, Samsung Galaxy Watch 4 on two subjects, and Polar Vantage M3 on two subjects. Subject age ranged between 11 and 76. Some subjects had their ECG was measured more than twice, and some with more than one smartwatch device. The Withings Scanwatch was having troubles finding the ECG signal with two subjects, requiring multiple attempts to get the successful recordings. The time difference between healthy baseline and the input ECG varied from 5 minutes to over 6 months. None of the subjects were experiencing MI during testing, therefore all the predictions are expected to not find any signs of infarction. The trained model however frequently predicted false positives (Table 4.1).

Huawei produces an ECG report with high image resolution, which makes the local thresholding in image processing step compute long. This resulted a waiting time of over 2 minutes and 30 seconds for the InfarctAPI response in InfarctWatch app. In contrast, InfarctAPI returned the response within 30 seconds with the ECG reports

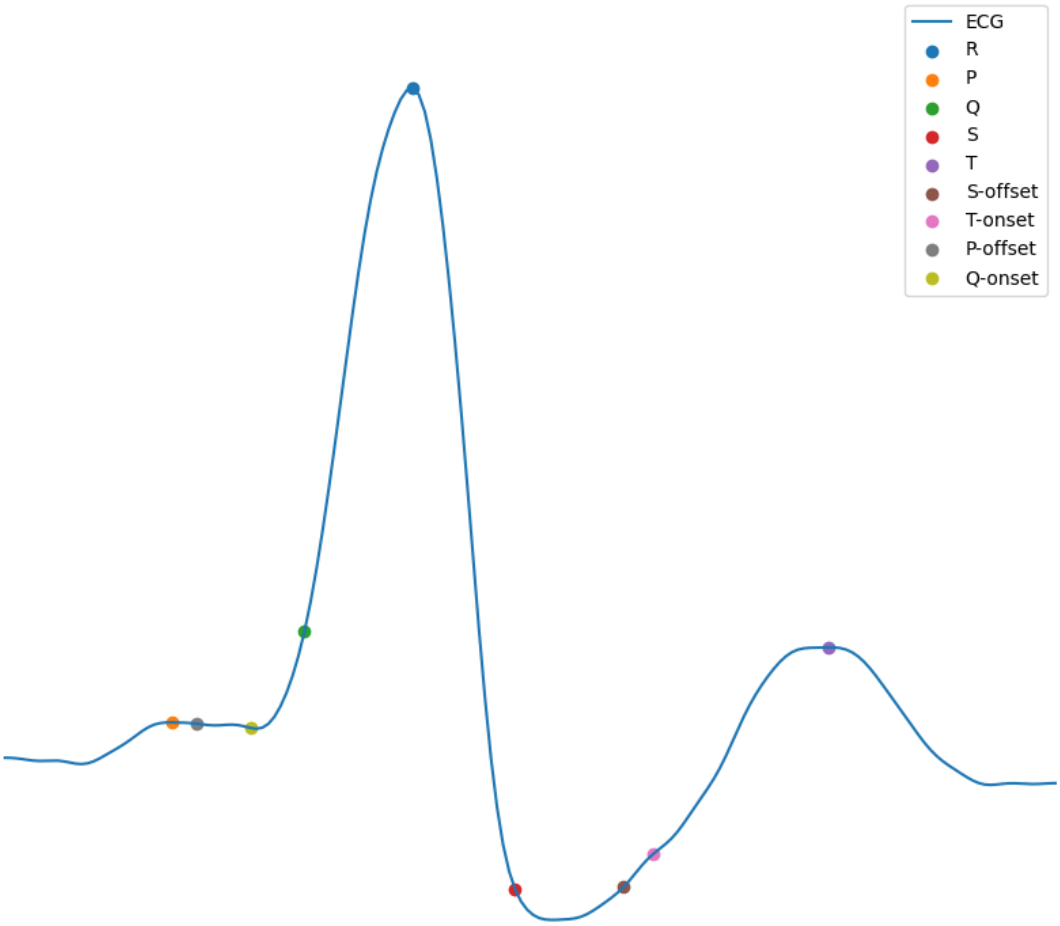

Figure 4.3: Detected ECG peaks and segments from Withings smartwatch ECG.

from other models. The peak and segment detection is demonstrated in Figure 4.3 and Figure 4.4, which displays one heart cycle peaks and segments from Withings and Huawei smartwatch ECG respectively. Figure 4.5, Figure 4.6 and Figure 4.7 displays an ECG segment from the report and its extracted ECG. The first two figures has prominent peaks and segments, but Figure 4.7 contains ECG recordings that could not be expected to have their peaks and segments detected accurately.

A second test was a usability test of the initial setup and the evaluation path in the InfarctWatch app (section 3.1). Only 4 subjects with age between 15 and 60 were

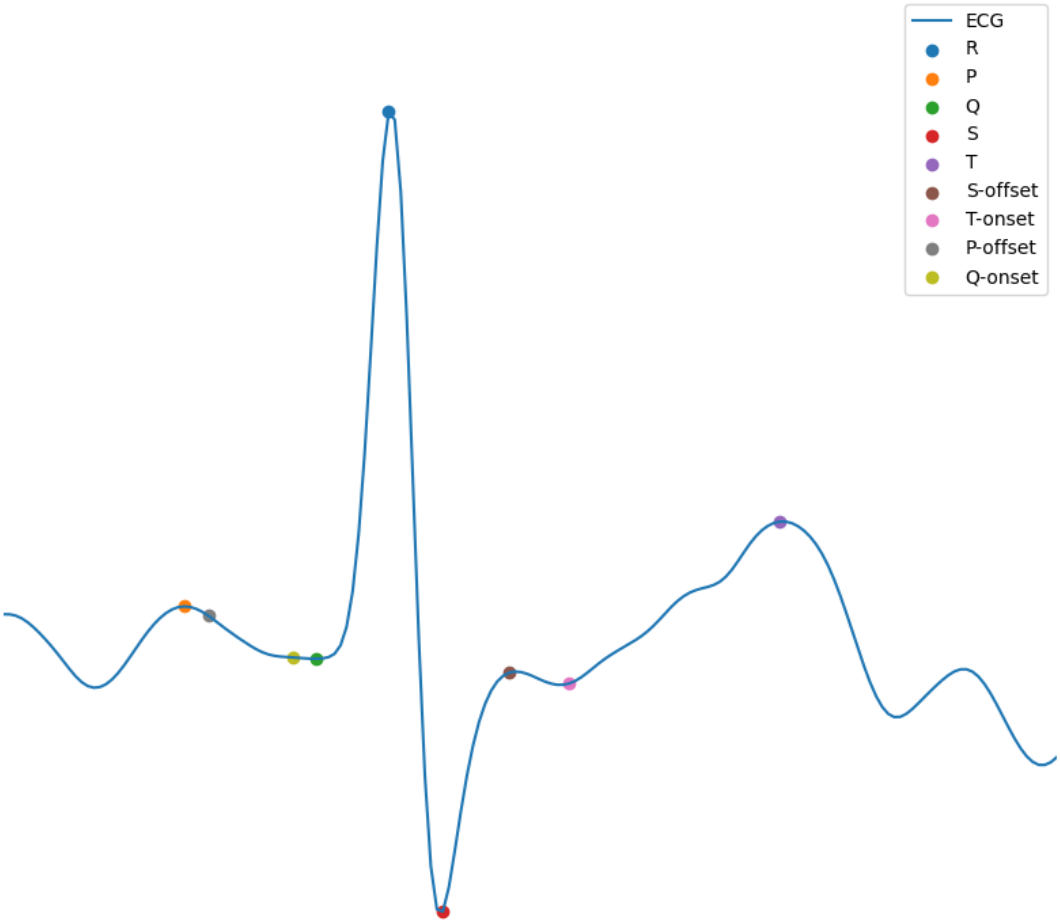

Figure 4.4: Detected ECG peaks and segments from Huawei smartwatch ECG.

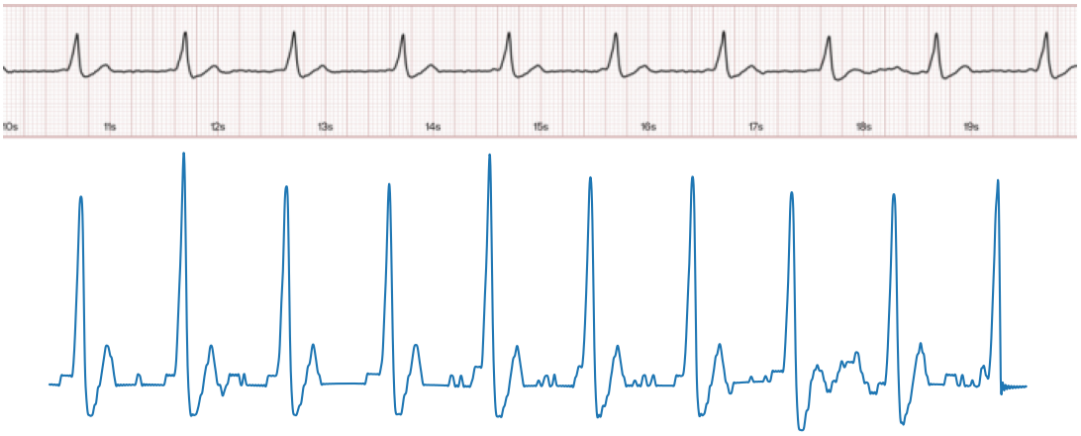

(a) Withings ScanWatch

(b) Huawei Watch Ultimate

Figure 4.5: Smartwatch ECG and extracted ECG signal 1/3

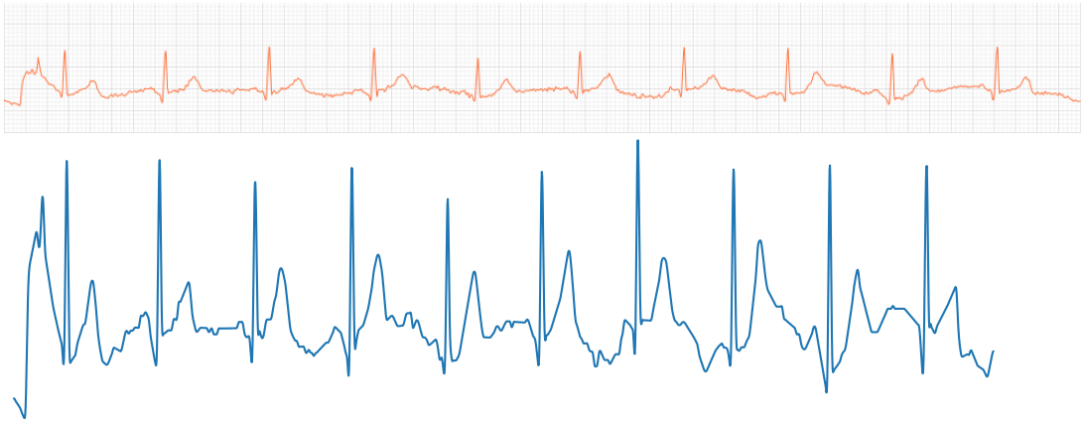

(a) Samsung Galaxy Watch 4

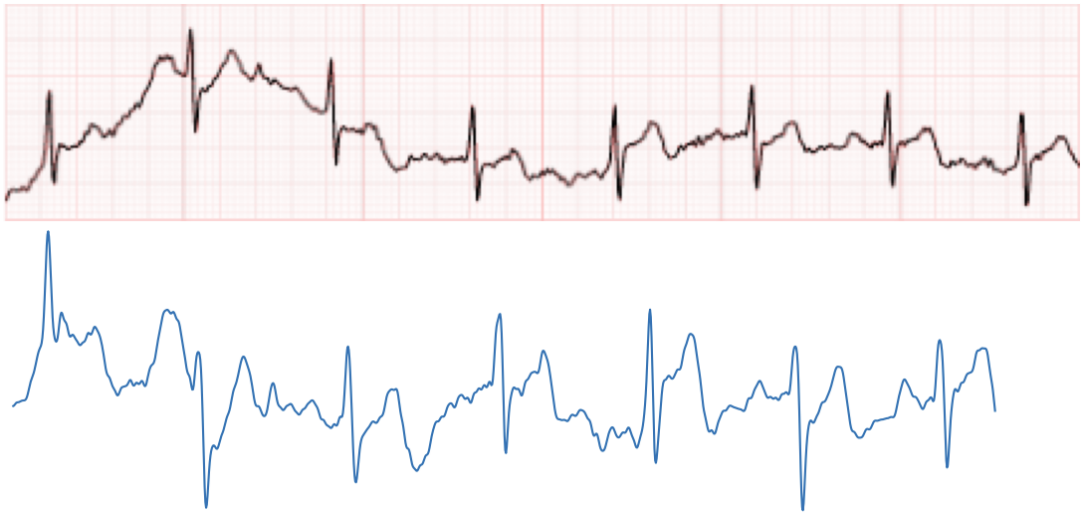

(b) Polar Vantage M3

Figure 4.6: Smartwatch ECG and extracted ECG signal 2/3

part of this test. Subjects performed the test alone but in supervision. First the subjects were trained how to measure the ECG and how to download the report to their phone, because none of them had prior experience with either smartwatches in general or those with ECG support. Because of their inexperience the supervisor helped subjects during the test how to find the ECG report from the companion app. Next, the supervisor tells the subject that they are in a scenario where they have just returned home from a doctor visit. The doctor told them that the subject is in risk of MI, and when they get back home they should install and open the InfarctWatch app and follow its instructions carefully. Also, the doctor had told

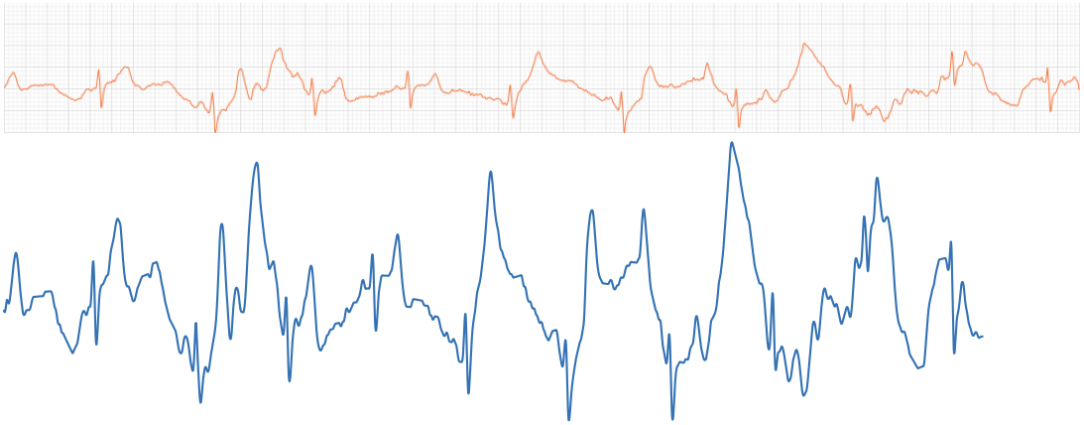

(a) Samsung Galaxy Watch 4

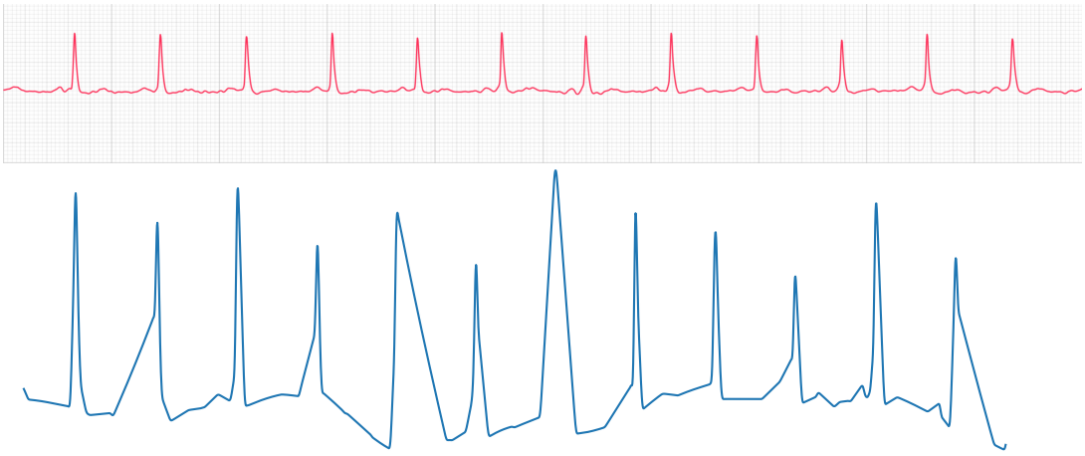

(b) Huawei Watch Ultimate

Figure 4.7: Smartwatch ECG and extracted ECG signal 3/3

that when they experience symptoms, the subject should record the ECG with their smartwatch and send it to InfarctWatch app for quick MI evaluation. The subject was then asked to open the InfarctWatch app for the first time. When the subject successfully succeeds to provide a healthy baseline ECG they are expected to ask the supervisor what to do next. The supervisor then tells that now the scenario changes. The next scenario is that several days have passed from the doctor visit, and the subject is experiencing weird symptoms which might relate with MI. The subject is then expected to measure their ECG again and send it to InfarctWatch app.

Subject	Age	Initial setup	Evaluation	Notes
1	60	success	success	Read instructions carefully. First thought the smartwatch continuously monitors their ECG. Was talking during measurement. In their opinion the process is too complex for elderly.
2	15	success	fail	Hardly read any instructions in the app.
3	34	success	fail	Hardly read any instructions in the app. Thought the app was stuck when it was waiting for the API response.
4	33	success	success	Read instructions carefully. Did not realize the initial setup was complete when app navigated to home view. In their opinion the process is too complex for elderly.

Table 4.2: Usability test results and notes.

As seen in Table 4.2, all subjects successfully completed the initial setup, but subjects number 2 and 3 did not ask supervisor anything after the initial setup, and completed the evaluation path with their first ECG assuming the test was fully completed. Subject number 1 asked what to do next after the initial setup, but also used their first ECG to complete the evaluation path. The subject did however realize this, and after they had confirmed their error with the supervisor they completed the evaluation again with a new ECG. Subject number 4 did not realize that the initial setup was completed after reaching the home page. Without asking what to do next, they completed the evaluation path with the first ECG. This subject did also realize this error and then asked what to do next. The subject completed the evaluation correctly with new ECG measurement. The general feedback was about the complexity of giving the ECG report file from the companion app to the InfarctWatch app.

5 Discussion

Thanks to the successful automated signal extraction, the InfarctWatch is functioning in a sense that the user is able to get their smartwatch ECG evaluated, but with poor prediction performance and on some cases with long evaluation waiting time. The process where the user downloads the ECG report from their smartwatch companion app, and then finding it from their phone's file system can be considered a difficult task for some users. Especially for the elderly, which is InfarctWatch's target group.

InfarctWatch is not receiving the same ECG that was captured from smartwatch ECG sensor, but instead from an image that is drawn into a PDF formatted ECG report file and the ECG signal is extracted from it. As mentioned in subsection 3.2.1, the image can differ considerably between providers meaning the amount of details the image has for the ECG signal is not in InfarctWatch control. Not only that, the model itself is not trained with smartwatch ECG, but with a medical grade lead I ECG sensor and with longer recording sessions. Asking for the multiple sequential smartwatch ECG measurements and combining them could possibly give more accurate predictions. The user interaction with the InfarctWatch was at the very start wanted to be as seamless as possible for its target group. Which is why compromises like sequential measurement, from the same lead or multiple, were omitted. Sequential ECG from multiple leads could have positive impact on the

model performance since there are not many studies that concludes a single lead to provide enough information for accurate infarction detection.

It is clear from the extracted smartwatch ECG segments which were show in Figure 4.5, Figure 4.6 and Figure 4.7 that each ECG is very different between both models and subjects. The peak and segment detection is assumed to be inaccurate in some signals due to their poor quality. The motion artifacts and poor sensor contact are the most relevant user related factors to signal quality. How the smartwatch ECG signal is preprocessed and drawn to the ECG report are the most important model related factors which affects the ECG signal InfarctWatch has access to. Because of all this, a well generalized preprocessing and extraction process to function with any model inevitably becomes a very challenging task. Instead of supporting any commercial smartwatch, one future development direction could be to develop an InfarctWatch smartwatch to solve user experience and ECG extraction related challenges. Alternatively, the modalities of different smartwatch providers and models could be solved by asking the user what is their smartwatch model in the InfarctWatch app. With this information, the whole pipeline in the InfarctAPI could make some smartwatch model specific adjustments. In addition, including more signals like the PPG from the wrist and have other wearables to provide seismocardiograph from the chest could help with improving the detection performance.

Even if the single lead is not enough to make medical professional resembling prediction performance in all AMI cases, it does not necessarily make the service insufficient for real world use. Hypothetically, if it is possible to detect a relevant portion out of all different AMI cases using only lead I signal, and the true positives would have relevant impact on patient delay while the false negatives does not make patient delay longer, it would mean the service overall would have high enough impact in reducing the patient delay. To make sure false negatives do not increase the patient

delay the app is specifically instructing its user to read app info page about AMI symptoms and seek medical attention regardless of the evaluation result if they are feeling any discomfort. The impact of the app guidance is also hypothetical and is not tested with AMI patients.

Another factor that is assumed to be relevant is the patient's adherence using the service. For example, if the detection performance is improved by adding more data as input with the sequential ECG measurement from different leads, it can make the service too complex for the patient and decrease their service adherence. Like with medical system delay improvements (subsection 2.2.1), it does not matter how well the InfarctWatch service is able to detect AMI, if most of its users do not even use it when they should. In pure statistical point of view, it is more relevant how many users are reached, and the ones with AMI are calling EMS faster after using the service, regardless of whether the service was able to detect AMI correctly or not. False positives are also important to analyze to make sure there are not too frequent false alarm situations, which can hinder the integrity of InfarctWatch and its use rate.

The hypothesis is that InfarctWatch could reduce the patient delay for AMI patients. In subsection 2.2.1, the factors that have been found to be relevant to patient delay duration were reviewed from multiple studies and summarized in Table 2.4. Also, other interventions to reduce patient delay were discussed and one meta-analysis was summarized in Table A.1. It could be speculated from these delay factors and expected intervention outcomes, that the InfarctWatch could potentially reduce patient delay for patients that identify their discomfort as possible AMI symptoms, but are still hesitant to call emergency medical service. InfarctWatch is expected to be most impactful for patients that delay the medical contact due to embarrassment and fear of bothering others in case of a false alarm. This is because the Infarct-

Watch is not involving any other human being, perceived seriousness of symptoms by detecting MI, AMI knowledge with the info page in the app, and FMC choice by instructing user to call the emergency number. Rasmussen, Munck, Kragstrup, *et al.* [57] found in their patient delay study of chest pain patients that the patient delay increased if patient had first consulted their symptoms by calling to a relative and reduced when calling to a non-relative. It is unknown how relevant is this finding among the 31% of patients in the study that were diagnosed AMI. If it were statistically relevant to AMI patients however, it could be seen as potential evidence that consulting a decision support system like the InfarctWatch may have significant impact to patient delay.

In retrospect the usability test was possibly too complex by having two scenarios, and the next scenario is requiring the subject to first ask for further instructions when they have nothing to do after the initial setup. This test could have been split into two occasions to test the setup and evaluation individually. Alternatively, the subjects could have been clearly told that they are expected to at some point ask the supervisor for further instructions when they feel they have nothing to do anymore. The subjects in the usability test were hoped to understand how InfarctWatch works as an additional service to the commercial smartwatch, apparently with too little information in the InfarctWatch app. This could be improved by adding more information to the initial setup path. For example by telling that the symptomless ECG is successfully saved, and in addition remind the user to quickly measure a new ECG when they feel symptoms and send it with the evaluation button in the home page.

6 Conclusion

The trained model had promising performance metrics when evaluating it with the test split. Unfortunately, since the real input data differs in nature a lot with the data used in training, the small scaled testing with commercial smartwatches resulted too many false positives to consider the trained model to be applicable for real world use. This data difference is seen as the most fundamental issue for InfarctWatch, and solving it should be in the highest priority in future development. Not only the data difference, but the ECG quality is compromised by extracting it from an image, measurement noise artifacts, and no guarantee of how accurately the image is drawn by its provider to be suitable for extraction in the first place. These issues indicate that the hypothesis of being able to train ML model to detect AMI from smartwatch ECG remains uncertain. Other high priority development steps should be improving and optimizing the image processing in InfarctAPI to support any model and to reduce computation time with high resolution images. In addition, solutions to have near seamless interaction between the InfarctWatch and the smartwatch, and clearer communication in the InfarctWatch app of how the service is working with their commercial smartwatch.

Regardless that the process of sending the smartwatch ECG to the service is not very user-friendly, and that the AMI detection performance is not sufficient the user is regardless able to get their smartwatch ECG extracted and processed for ML

prediction. In addition, ECG reports from four different smartwatch models and four different providers were successfully evaluated. InfarctWatch showed positive light regarding the questions of is it possible to make a AMI detection service that uses commercial smartwatch ECG (1), and could it support multiple providers (3). The question (2) whether it is possible to work as third party service InfarctWatch had to make a lot of compromises to have streamlined but complex process of sending the ECG file from the smartwatch companion app to InfarctWatch app. InfarctWatch also did not have access to the raw ECG sensor data as a third party service. The concept InfarctWatch envisions is believed to be relevant in reducing patient delay, but this thesis did not provide any relevant statistical evidence towards it. InfarctWatch is in a good starting point towards the concept of remote healthcare supporting tool for AMI patients, and hopefully further exploration of this concept emerges to the world in the future.

References

[1] World Health Organization, *Cardiovascular diseases (cvds)*, https://www.who.int/news-room/fact-sheets/detail/cardiovascular-diseases-(cvds), Accessed: 2025-09-24, 2025.

[2] Institute for Health Metrics and Evaluation (IHME), "Global burden of disease 2021: Findings from the gbd 2021 study", Institute for Health Metrics and Evaluation (IHME), Seattle, WA, Tech. Rep., 2024, Accessed: 2025-09-24. [Online]. Available: https://www.healthdata.org/research-analysis/library/global-burden-disease-2021-findings-gbd-2021-study.

[3] OECD, *Health at a glance 2023* (Health at a glance), en. OECD, Nov. 2023, ch. 6. [Online]. Available: https://www.oecd.org/en/publications/health-at-a-glance-2023_7a7afb35-en/full-report/mortality-following-acute-myocardial-infarction-ami_999cd0f3.html#indicator-d1e27536-8fd3aa50e4.

[4] F. Zijlstra, A. Patel, M. Jones, *et al.*, "Clinical characteristics and outcome of patients with early (4 h) presentation treated by primary coronary angioplasty or thrombolytic therapy for acute myocardial infarction", en, *Eur. Heart J.*, vol. 23, no. 7, pp. 550–557, Apr. 2002.

[5] C. M. Gibson, S. A. Murphy, A. J. Kirtane, *et al.*, "Association of duration of symptoms at presentation with angiographic and clinical outcomes after fibri-

nolytic therapy in patients with ST-segment elevation myocardial infarction", en, *J. Am. Coll. Cardiol.*, vol. 44, no. 5, pp. 980–987, Sep. 2004.

[6] K. Wechkunanukul, H. Grantham, and R. A. Clark, "Global review of delay time in seeking medical care for chest pain: An integrative literature review", en, *Aust. Crit. Care*, vol. 30, no. 1, pp. 13–20, Jan. 2017.

[7] P. Assantachai, "Concerted actions toward healthy ageing in ASEAN countries", *Siriraj Med. J.*, vol. 73, no. 9, pp. 633–634, Sep. 2021.

[8] W. E. Boden, R. De Caterina, J. C. Kaski, *et al.*, "Myocardial ischemic syndromes: A new nomenclature to harmonize evolving international clinical practice guidelines", en, *Circulation*, vol. 150, no. 20, pp. 1631–1637, Nov. 2024.

[9] J. Sandelin, *Identification of myocardial infarction by high-frequency serial ECG measurement - UTUPub — urn.fi*, `https://urn.fi/URN:NBN:fi-fe2022041929460`, [Accessed 19-02-2026], 2022.

[10] C. Han, Y. Song, H.-S. Lim, *et al.*, "Automated detection of acute myocardial infarction using asynchronous electrocardiogram signals-preview of implementing artificial intelligence with multichannel electrocardiographs obtained from smartwatches: Retrospective study", en, *J. Med. Internet Res.*, vol. 23, no. 9, e31129, Sep. 2021.

[11] J.-H. Choi, S.-H. Song, H. Kim, *et al.*, "Machine learning algorithm to predict atrial fibrillation using serial 12-lead ECGs based on left atrial remodeling", en, *J. Am. Heart Assoc.*, vol. 13, no. 19, e034154, Oct. 2024.

[12] A. Sbrollini, M. C. De Jongh, C. C. Ter Haar, *et al.*, "Serial electrocardiography to detect newly emerging or aggravating cardiac pathology: A deep-learning approach", en, *Biomed. Eng. Online*, vol. 18, no. 1, p. 15, Feb. 2019.

[13] R. Hirani, K. Noruzi, H. Khuram, *et al.*, "Artificial intelligence and healthcare: A journey through history, present innovations, and future possibilities", en, *Life (Basel)*, vol. 14, no. 5, p. 557, Apr. 2024.

[14] A. A. Abahussin, "Perceived impact of wearable fitness trackers on health behaviours in saudi adults", en, *Healthcare (Basel)*, vol. 14, no. 1, p. 126, Jan. 2026.

[15] N. Kumar, *Smartwatch Statistics (2026) – Global Users & Market Share — demandsage.com*, `https://www.demandsage.com/smartwatch-statistics`, [Accessed 09-02-2026].

[16] C. Köhler, A. Bartschke, D. Fürstenau, T. Schaaf, and E. Salgado-Baez, "The value of smartwatches in the health care sector for monitoring, nudging, and predicting: Viewpoint on 25 years of research", en, *J. Med. Internet Res.*, vol. 26, e58936, Oct. 2024.

[17] J. Medina-Avelino, R. Silva-Bustillos, and J. A. Holgado-Terriza, "Are wearable ECG devices ready for hospital at home application?", en, *Sensors (Basel)*, vol. 25, no. 10, p. 2982, May 2025.

[18] A. Samol, K. Bischof, B. Luani, D. Pascut, M. Wiemer, and S. Kaese, "Recording of bipolar multichannel ECGs by a smartwatch: Modern ECG diagnostic 100 years after einthoven", en, *Sensors (Basel)*, vol. 19, no. 13, p. 2894, Jun. 2019.

[19] J. Choi, J. Kim, C. Spaccarotella, *et al.*, "Smartwatch ECG and artificial intelligence in detecting acute coronary syndrome compared to traditional 12-lead ECG", en, *Int. J. Cardiol. Heart Vasc.*, vol. 56, no. 101573, p. 101 573, Feb. 2025.

[20] *Rubber duck debugging - Wikipedia — en.wikipedia.org*, `https://en.wikipedia.org/wiki/{R}ubber_duck_debugging`, [Accessed 07-04-2026].

[21] I. Rehman and A. Rehman, "Anatomy, thorax, heart", en, in *StatPearls*, Treasure Island (FL): StatPearls Publishing, Jan. 2025.

[22] Y. Wapcaplet, *File:Diagram of the human heart.svg - Wikimedia Commons — commons.wikimedia.org*, https://commons.wikimedia.org/wiki/File:Diagram_of_the_human_heart.svg, [Accessed 15-12-2025].

[23] M. Sampson and A. McGrath, "Understanding the ECG. part 1: Anatomy and physiology", en, *Br. J. Card. Nurs.*, vol. 10, no. 11, pp. 548–554, Nov. 2015.

[24] *File:De-Conduction ap.png - ECGpedia — en.ecgpedia.org*, https://en.ecgpedia.org/wiki/File:De-Conduction_ap.png, [Accessed 11-12-2025].

[25] Z. Kotsialou, N. Makris, and S. Gall, "Fundamentals of the electrocardiogram and common cardiac arrhythmias", en, *Anaesth. Intensive Care Med.*, vol. 25, no. 3, pp. 219–222, Mar. 2024.

[26] *File:EKG leads.png - Wikimedia Commons — commons.wikimedia.org*, https://commons.wikimedia.org/wiki/File:EKG_leads.png, [Accessed 11-12-2025].

[27] *File:Limb leads of EKG.png - Wikimedia Commons — commons.wikimedia.org*, https://commons.wikimedia.org/wiki/File:Limb_leads_of_EKG.png, [Accessed 11-12-2025].

[28] *U Wave — litfl.com*, https://litfl.com/u-wave-ecg-library/, [Accessed 11-12-2025].

[29] E. A. Ashley and J. Niebauer, *Chapter 3, Conquering the ECG*, en. London, England: REMEDICA, 2004.

[30] M. Sampson and A. McGrath, "Understanding the ECG part 2: ECG basics", en, *Br. J. Card. Nurs.*, vol. 10, no. 12, pp. 588–594, Dec. 2015.

[31] F. Luzza, F. Catanzariti, M. Navarra, and P. Pugliatti, "U wave manifesting in alternating beats: The bigeminal U wave", en, *J. Electrocardiol.*, vol. 92, no. 154092, p. 154 092, Sep. 2025.

[32] K. Thygesen, J. S. Alpert, A. S. Jaffe, *et al.*, "Fourth universal definition of myocardial infarction (2018)", en, *J. Am. Coll. Cardiol.*, vol. 72, no. 18, pp. 2231–2264, Oct. 2018.

[33] M. Q. Leong, C. W. Lim, and Y. F. Lai, "Comparison of Hospital-at-Home models: A systematic review of reviews", en, *BMJ Open*, vol. 11, no. 1, e043285, Jan. 2021.

[34] N. M. de Vries, A. Zepeda-Echavarria, R. R. van de Leur, *et al.*, "Detection of ischemic ST-segment changes using a novel handheld ECG device in a porcine model", en, *JACC Adv.*, vol. 2, no. 5, p. 100 410, Jul. 2023.

[35] M. Jabara and A. Sharma, "A step forward in prehospital electrocardiogram development", en, *JACC Adv.*, vol. 2, no. 5, p. 100 441, Jul. 2023.

[36] N. Salari, F. Morddarvanjoghi, A. Abdolmaleki, *et al.*, "The global prevalence of myocardial infarction: A systematic review and meta-analysis", en, *BMC Cardiovasc. Disord.*, vol. 23, no. 1, p. 206, Apr. 2023.

[37] G. A. Mensah, V. Fuster, C. J. L. Murray, G. A. Roth, and Global Burden of Cardiovascular Diseases and Risks Collaborators, "Global burden of cardiovascular diseases and risks, 1990-2022", en, *J. Am. Coll. Cardiol.*, vol. 82, no. 25, pp. 2350–2473, Dec. 2023.

[38] B. E. Landon, L. A. Hatfield, P. Bakx, *et al.*, "Differences in treatment patterns and outcomes of acute myocardial infarction for low- and high-income patients in 6 countries", en, *JAMA*, vol. 329, no. 13, pp. 1088–1097, Apr. 2023.

[39] J. L. M. Björkegren and A. J. Lusis, "Atherosclerosis: Recent developments", en, *Cell*, vol. 185, no. 10, pp. 1630–1645, May 2022.

[40] L. Badimon and G. Vilahur, "Thrombosis formation on atherosclerotic lesions and plaque rupture", en, *J. Intern. Med.*, vol. 276, no. 6, pp. 618–632, Dec. 2014.

[41] *All about myocardial infarction: STEMI vs NSTEMI — lonestarneurology.net*, https://lonestarneurology.net/blog/myocardial-infarction-stemi-vs-nstemi/, [Accessed 08-12-2025].

[42] *Do You Know the Symptoms of a Heart Attack? — my.clevelandclinic.org*, https://my.clevelandclinic.org/health/diseases/16818-heart-attack-myocardial-infarction, [Accessed 08-12-2025].

[43] *Percutaneous Coronary Intervention (PCI) — my.clevelandclinic.org*, https://my.clevelandclinic.org/health/treatments/22066-percutaneous-coronary-intervention, [Accessed 08-12-2025].

[44] *What Is CABG? — my.clevelandclinic.org*, https://my.clevelandclinic.org/health/treatments/16897-coronary-artery-bypass-surgery, [Accessed 08-12-2025].

[45] W. Guan, A. K. Venkatesh, X. Bai, *et al.*, "Time to hospital arrival among patients with acute myocardial infarction in china: A report from china PEACE prospective study", *Eur. Heart J. Qual. Care Clin. Outcomes*, vol. 5, no. 1, pp. 63–71, Jan. 2019.

[46] T. Toshima, A. Hirayama, T. Watanabe, *et al.*, "Unmet needs for emergency care and prevention of prehospital death in acute myocardial infarction", en, *J. Cardiol.*, vol. 77, no. 6, pp. 605–612, Jun. 2021.

[47] K. Dai, N. Shiode, and Y. Nakano, "Treatment delays in patients with acute myocardial infarction", en, *Circ. J.*, vol. 86, no. 4, pp. 609–610, Mar. 2022.

[48] L. Neubeck and A. Maiorana, "Time to get help? acute myocardial infarction and delay in calling an ambulance", en, *Heart Lung Circ.*, vol. 24, no. 1, pp. 1–3, Jan. 2015.

[49] A. Guerchicoff, S. J. Brener, A. Maehara, *et al.*, "Impact of delay to reperfusion on reperfusion success, infarct size, and clinical outcomes in patients with ST-segment elevation myocardial infarction: The INFUSE-AMI trial (INFUSE-Anterior myocardial infarction)", en, *JACC Cardiovasc. Interv.*, vol. 7, no. 7, pp. 733–740, Jul. 2014.

[50] B. Redfors, R. Mohebi, G. Giustino, *et al.*, "Time delay, infarct size, and microvascular obstruction after primary percutaneous coronary intervention for ST-segment-elevation myocardial infarction", en, *Circ. Cardiovasc. Interv.*, vol. 14, no. 2, e009879, Feb. 2021.

[51] R. V. Luepker, J. M. Raczynski, S. Osganian, *et al.*, "Effect of a community intervention on patient delay and emergency medical service use in acute coronary heart disease", *JAMA*, vol. 284, no. 1, p. 60, Jul. 2000.

[52] P. Widimský, P. Kala, and R. Rokyta, "Summary of the 2012 ESC guidelines for the management of acute myocardial infarction in patients presenting with ST-segment elevations. prepared by the czech society of cardiology", en, *Cor Vasa*, vol. 54, no. 9-10, e273–e289, Sep. 2012.

[53] D. Garrido, D. Petrova, A. Catena, J. A. Ramírez-Hernández, and R. Garcia-Retamero, "Recognizing a heart attack: Patients' knowledge of cardiovascular risk factors and its relation to prehospital decision delay in acute coronary syndrome", *Front. Psychol.*, vol. 11, Aug. 2020.

[54] T. Caltabellotta, J. Magne, B. Salerno, *et al.*, "Characteristics associated with patient delay during the management of ST-segment elevated myocardial in-

farction, and the influence of awareness campaigns", en, *Arch. Cardiovasc. Dis.*, vol. 114, no. 4, pp. 305–315, Apr. 2021.

[55] H.-S. Kim, K.-S. Lee, S. J. Eun, *et al.*, "Gender differences in factors related to prehospital delay in patients with ST-segment elevation myocardial infarction", en, *Yonsei Med. J.*, vol. 58, no. 4, p. 710, 2017.

[56] F. Rivero, T. Bastante, J. Cuesta, *et al.*, "Factors associated with delays in seeking medical attention in patients with ST-segment elevation acute coronary syndrome", en, *Rev. Esp. Cardiol. (Engl. Ed.)*, vol. 69, no. 3, pp. 279–285, Mar. 2016.

[57] C.-H. Rasmussen, A. Munck, J. Kragstrup, and T. Haghfelt, "Patient delay from onset of chest pain suggesting acute coronary syndrome to hospital admission", en, *Scand. Cardiovasc. J.*, vol. 37, no. 4, pp. 183–186, Sep. 2003.

[58] V. C. K. Venkatesan, S. Madhavi, S. K. R, and K. P, "A study to explore the factors related to treatment seeking delay among adults diagnosed with acute myocardial infarction at KMCH, coimbatore", en, *Indian Heart J.*, vol. 70, no. 6, pp. 793–801, Nov. 2018.

[59] I. Z. Chowdhury, M. N. Amin, M. Z. Chowdhury, S. M. Rahman, M. Ahmed, and F. A. Cader, "Pre hospital delay and its associated factors in acute myocardial infarction in a developing country", en, *PLoS One*, vol. 16, no. 11, e0259979, Nov. 2021.

[60] A. Kumar, A. Sanghera, B. Sanghera, *et al.*, "Chest pain symptoms during myocardial infarction in patients with and without diabetes: A systematic review and meta-analysis", en, *Heart*, vol. 109, no. 20, pp. 1516–1524, Sep. 2023.

[61] H. Alshahrani, R. McConkey, J. Wilson, M. Youssef, and D. Fitzsimons, "Female gender doubles pre-hospital delay times for patients experiencing ST seg-

ment elevation myocardial infarction in saudi arabia", en, *Eur. J. Cardiovasc. Nurs.*, vol. 13, no. 5, pp. 399–407, Oct. 2014.

[62] F. C. Mussi, A. S. Mendes, T. L. d. Queiroz, A. L. S. Costa, Á. Pereira, and B. Caramelli, "Pre-hospital delay in acute myocardial infarction: Judgement of symptoms and resistance to pain", en, *Rev. Assoc. Med. Bras.*, vol. 60, no. 1, pp. 63–69, Jan. 2014.

[63] M. M. Ottesen, U. Dixen, C. Torp-Pedersen, and L. Køber, "Prehospital delay in acute coronary syndrome–an analysis of the components of delay", en, *Int. J. Cardiol.*, vol. 96, no. 1, pp. 97–103, Jul. 2004.

[64] A. Alishahi Tabriz, M.-R. Sohrabi, N. Kiapour, and S. Yazdani, "Factors associated with delay in thrombolytic therapy in patients with ST-elevation myocardial infarction", en, *J. Tehran Heart Cent.*, vol. 7, no. 2, pp. 65–71, May 2012.

[65] L. Perkins-Porras, D. L. Whitehead, P. C. Strike, and A. Steptoe, "Pre-hospital delay in patients with acute coronary syndrome: Factors associated with patient decision time and home-to-hospital delay", en, *Eur. J. Cardiovasc. Nurs.*, vol. 8, no. 1, pp. 26–33, Mar. 2009.

[66] D. M. Taylor, D. Garewal, M. Carter, M. Bailey, and A. Aggarwal, "Factors that impact upon the time to hospital presentation following the onset of chest pain", en, *Emerg. Med. Australas.*, vol. 17, no. 3, pp. 204–211, Jun. 2005.

[67] H. Yan, L. Song, J. Yang, Y. Sun, and D. Hu, "The association between pre-infarction angina and care-seeking behaviors and its effects on early reperfusion rates for acute myocardial infarction", en, *Int. J. Cardiol.*, vol. 135, no. 1, pp. 86–92, Jun. 2009.

[68] S. Banharak, A. Metprommarat, W. Mahikul, T. Jeamjitvibool, and A. Karaket, "Effectiveness of acute myocardial infarction interventions on selected out-

comes among community dwelling-older adults: A systematic review and meta-analysis", en, *Sci. Rep.*, vol. 13, no. 1, p. 18 538, Oct. 2023.

[69] A. B. Teixeira, L. F. Zancaner, F. F. d. F. Ribeiro, *et al.*, "Otimização da terapia de reperfusão no infarto agudo do miocárdio com supradesnível do segmento ST por meio de telemedicina baseada no WhatsApp®", en, *Arq. Bras. Cardiol.*, vol. 118, no. 3, pp. 556–564, Mar. 2022.

[70] B. Farquharson, M. Johnston, B. Williams, *et al.*, "Reducing patient delay in acute coronary syndrome: Randomized controlled trial testing effect of behaviour change intervention on intentions to seek help", en, *Br. J. Health Psychol.*, vol. 28, no. 1, pp. 188–207, Feb. 2023.

[71] W.-C. Liu, C.-S. Lin, C.-S. Tsai, *et al.*, "A deep learning algorithm for detecting acute myocardial infarction", en, *EuroIntervention*, vol. 17, no. 9, pp. 765–773, Oct. 2021.

[72] Y. Zhao, J. Xiong, Y. Hou, *et al.*, "Early detection of ST-segment elevated myocardial infarction by artificial intelligence with 12-lead electrocardiogram", en, *Int. J. Cardiol.*, vol. 317, pp. 223–230, Oct. 2020.

[73] J. P. Martínez, O. Pahlm, M. Ringborn, S. Warren, P. Laguna, and L. Sornmo, "The STAFF III database: ECGs recorded during acutely induced myocardial ischemia", Sep. 2017.

[74] P. Laguna and L. Sörnmo, "The STAFF III ECG database and its significance for methodological development and evaluation", en, *J. Electrocardiol.*, vol. 47, no. 4, pp. 408–417, Jul. 2014.

[75] A. Aranda, P. Bonizzi, J. Karel, and R. Peeters, "Acute MI detection derived from ECG parameters distribution", in *2019 Computing in Cardiology Conference (CinC)*, Computing in Cardiology, Dec. 2019.

[76] R. Brisk, R. Bond, D. Finlay, *et al.*, "The effect of confounding data features on a deep learning algorithm to predict complete coronary occlusion in a retrospective observational setting", en, *Eur. Heart J. Digit. Health*, vol. 2, no. 1, pp. 127–134, Mar. 2021.

[77] J. Lehmacher, J. T. Neumann, N. A. Sörensen, *et al.*, "Predictive value of serial ECGs in patients with suspected myocardial infarction", en, *J. Clin. Med.*, vol. 9, no. 7, p. 2303, Jul. 2020.

[78] S. Shalev-Shwartz and S. Ben-David, *Understanding machine learning*. Cambridge, England: Cambridge University Press, May 2014.

[79] A. Jung, *Machine Learning: The Basics*. Singapore: Springer, 2022.

[80] *File:Neural network bottleneck achitecture.svg - Wikimedia Commons — commons.wikimedia.org*, `https://commons.wikimedia.org/wiki/File:Neural_network_bottleneck_achitecture.svg`, [Accessed 22-01-2026].

[81] R. C. Gonzalez and R. E. Woods, *Digital Image Processing*, 3rd ed. Upper Saddle River, NJ: Pearson, Aug. 2007.

[82] *Skimage.filters — skimage 0.26.0 documentation — scikit-image.org*, `https://scikit-image.org/docs/stable/api/skimage.filters.html#skimage.filters.threshold_local`, [Accessed 13-03-2026].

[83] *George B. Moody PhysioNet Challenge — moody-challenge.physionet.org*, `https://moody-challenge.physionet.org/2024/`, [Accessed 18-03-2026].

[84] J. D. Fortune, N. E. Coppa, K. T. Haq, H. Patel, and L. G. Tereshchenko, "Digitizing ECG image: A new method and open-source software code", en, *Comput. Methods Programs Biomed.*, vol. 221, no. 106890, p. 106 890, Jun. 2022.

[85] *File:Premature SVC.jpg - Wikipedia — en.wikipedia.org*, `en.wikipedia.org/wiki/{F}ile:{P}remature_{S}{V}{C}.jpg`, [Accessed 13-02-2026].

[86] *Voltage Calibration of the ECG — ecgbook.com*, https://www.ecgbook.com/ecg-calibration/#4, [Accessed 17-02-2026].

[87] J. Pan and W. J. Tompkins, "A real-time QRS detection algorithm", en, *IEEE Trans. Biomed. Eng.*, vol. 32, no. 3, pp. 230–236, Mar. 1985.

[88] *Find_peaks — SciPy v1.17.0 Manual — docs.scipy.org*, https://docs.scipy.org/doc/scipy/reference/generated/scipy.signal.find_peaks.html, [Accessed 26-02-2026].

[89] P. Laguna, R. G. Mark, A. L. Goldberger, and G. B. Moody, *The QT database*, 1997.

[90] M. Barandas, D. Folgado, L. Fernandes, *et al.*, "TSFEL: Time series feature extraction library", en, *SoftwareX*, vol. 11, no. 100456, p. 100 456, Jan. 2020.

[91] J. Lázaro, A. Alcaine, D. Romero, *et al.*, "Electrocardiogram derived respiratory rate from QRS slopes and r-wave angle", en, *Ann. Biomed. Eng.*, vol. 42, no. 10, pp. 2072–2083, Oct. 2014.

[92] *RobustScaler — scikit-learn.org*, https://scikit-learn.org/stable/modules/generated/sklearn.preprocessing.{R}obust{S}caler.html, [Accessed 09-03-2026].

[93] *3.4. Metrics and scoring: Quantifying the quality of predictions — scikit-learn.org*, https://scikit-learn.org/stable/modules/model_evaluation.html#balanced-accuracy-score, [Accessed 09-03-2026].

Appendix A AMI intervention categories

Intervention	Expected outcomes	Description
Direct mail	To reduce fear, embarrassment and feel of bother	Mail sent every two months with a core message of the responsibility to seek help at onset of symptoms by either patient themselves or their relative. Relative responsibility was expected to reduce embarrassment and feel of bother.
Community based intervention	To reduce out of hospital delays	Alternating AMI topics campaigned by various multimedia channels and healthcare professionals. Topics were: AMI awareness and rapid actions, development of heart attack plan, AMI for women, variability of AMI symptoms, bystander response to MI and use of emergency number.
Multi-component strategies & group health education	Improve AMI survival, symptom recognition and calling fast to EMS	Initial meeting with patient, relatives and healthcare. Followed by four interventions: Local advisory group in healthcare, 18 month education program for patient, AMI education to healthcare professionals and education by physician for risk patient.
Heart Attack Survival Kit (HASK) & firefighters	Increase use of EMS and 911 for AMI symptoms, taking aspirin for chest pain	HASK is an easily placeable, red cardboard info sheet about warning signs of AMI, recommendation to call EMS or 911 and take aspirin for chest pain. To promote use of 911, local firefighters delivered the HASK to the door.
Tailored educational/-counseling intervention	Improved AMI knowledge, attitude, belief. Also, to increase use of 911 and EMS and to reduce anxiety.	Intervention contained information about pathophysiology of AMI, symptoms of AMI, prompt response, appropriate actions for AMI, rehearsal plan and take-home questions.
Structured education and counseling intervention	Same as tailored educational/-counseling intervention	Multi step program: Detailed educational and counseling, education of atypical symptoms and actions at onset of AMI symptoms, participants were asked to repeat given information and lastly 30 to 60 min one-to-one session.
Tricked intervention promoting memory and concern	Promote older female memory and concern	Using abbreviation with keywords like FACCTS (Fatigue, Anxiety, Chest discomfort, Tummy, Shortness of breath and Sleeping difficulties) and CURB (Chest sensation or pain, Unusual fatigue, Pain radiating back, jaw or arm pain, and Breathing difficulties).
A nurse-based case management	Reduce AMI mortality, readmission, patient delay and anxiety	Frequent home visits and telephone calls by nurse to detect problems or risks and to give advice like symptom management and medication use.

Table A.1: Summary of AMI intervention categories identified by Banharak, Metprommarat, Mahikul, *et al.* [68] based on their review of 11 primary studies

Appendix B Huawei ECG report to signal

Figure B.1: Cropped ECG report from Huawei smartwatch

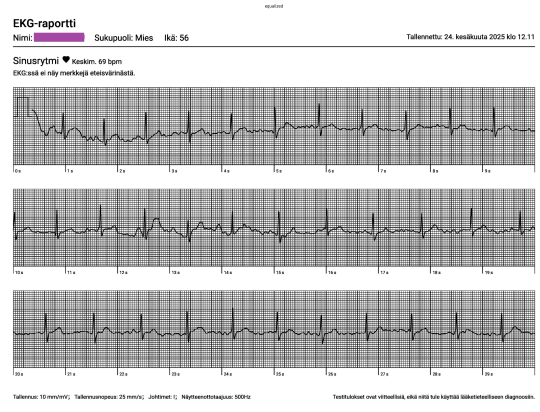

(a) Greyscaled and histogram equalized

(b) Binary image using local thresholding

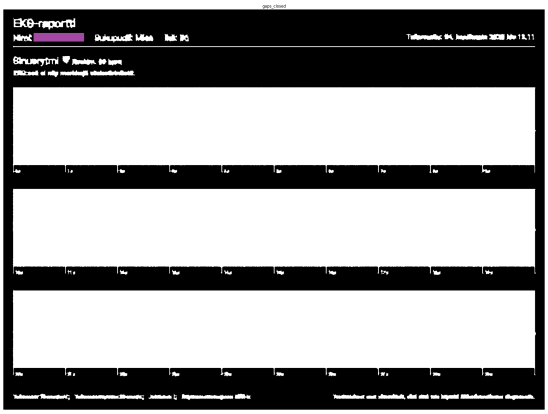

(c) Gap closing

(d) Opening with large structuring element

Figure B.2: Cropped Huawei ECG report processed by grid detection algorithm

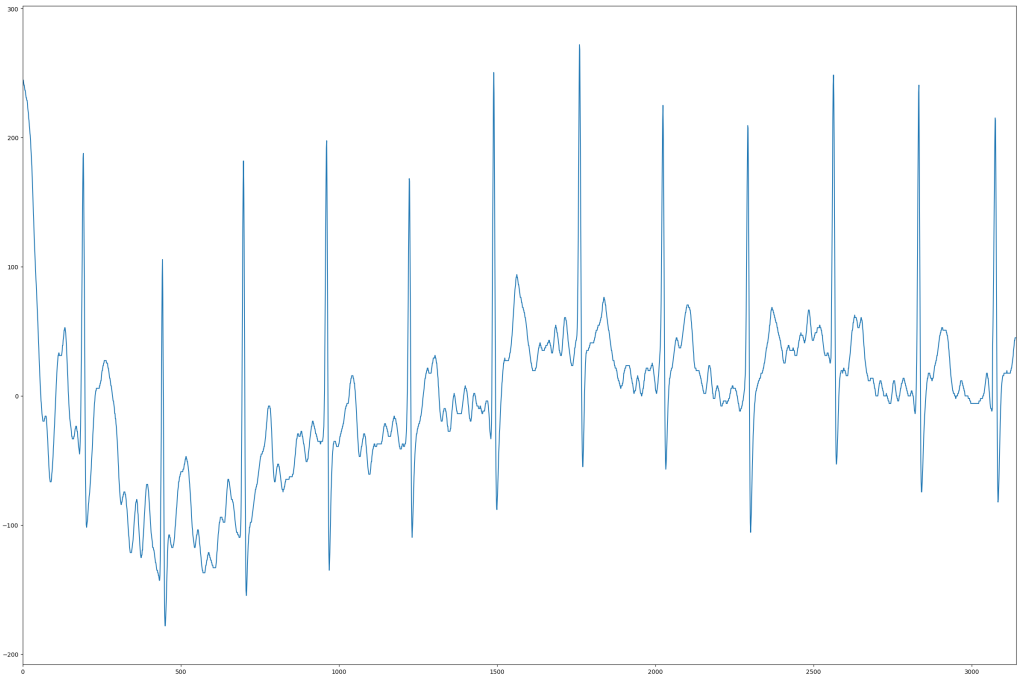

Figure B.3: First 10 seconds of the extracted ECG signal

Appendix C Feature differences in ML modeling step

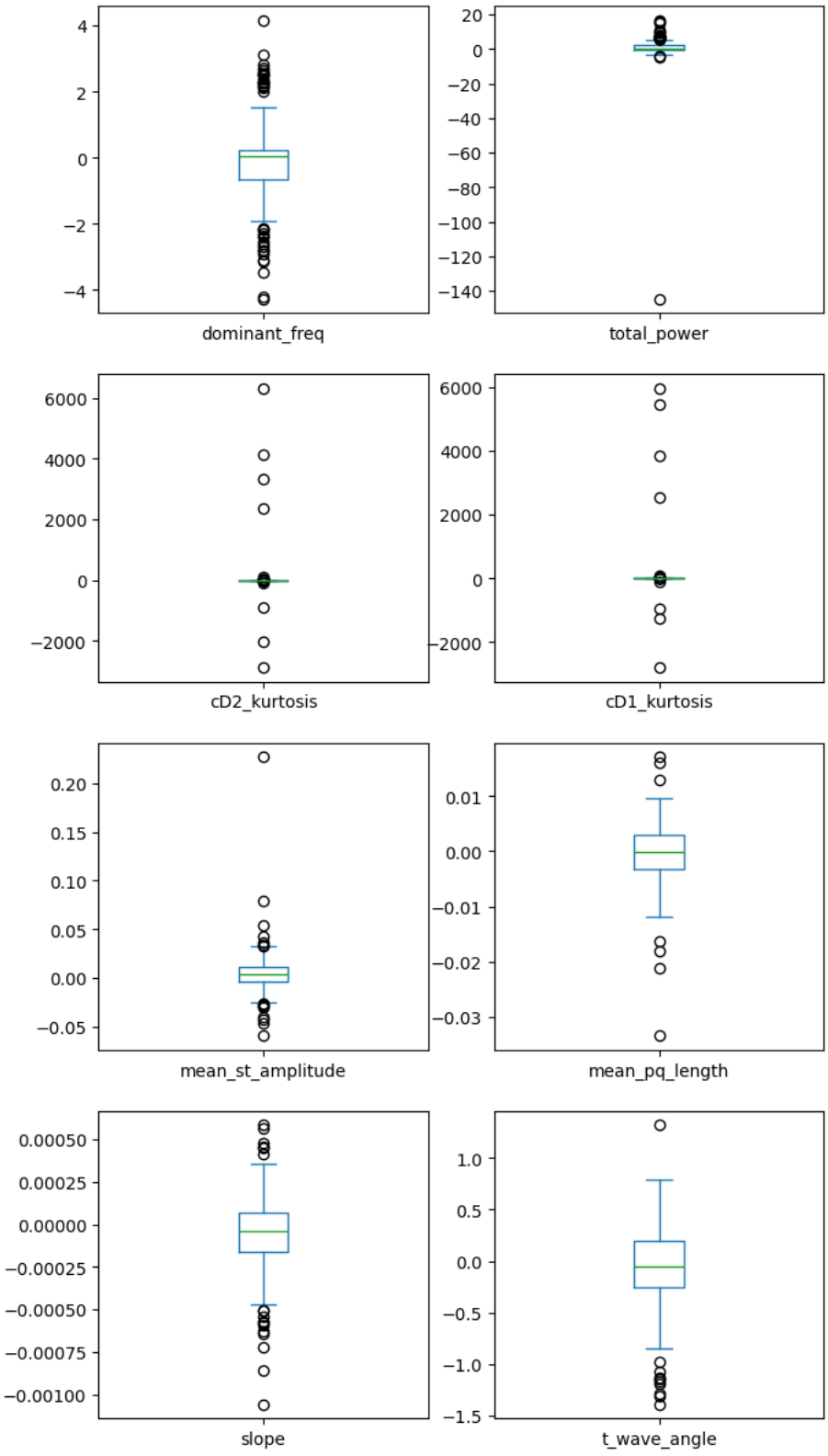

Figure C.1: Box plots of feature differences 1/2

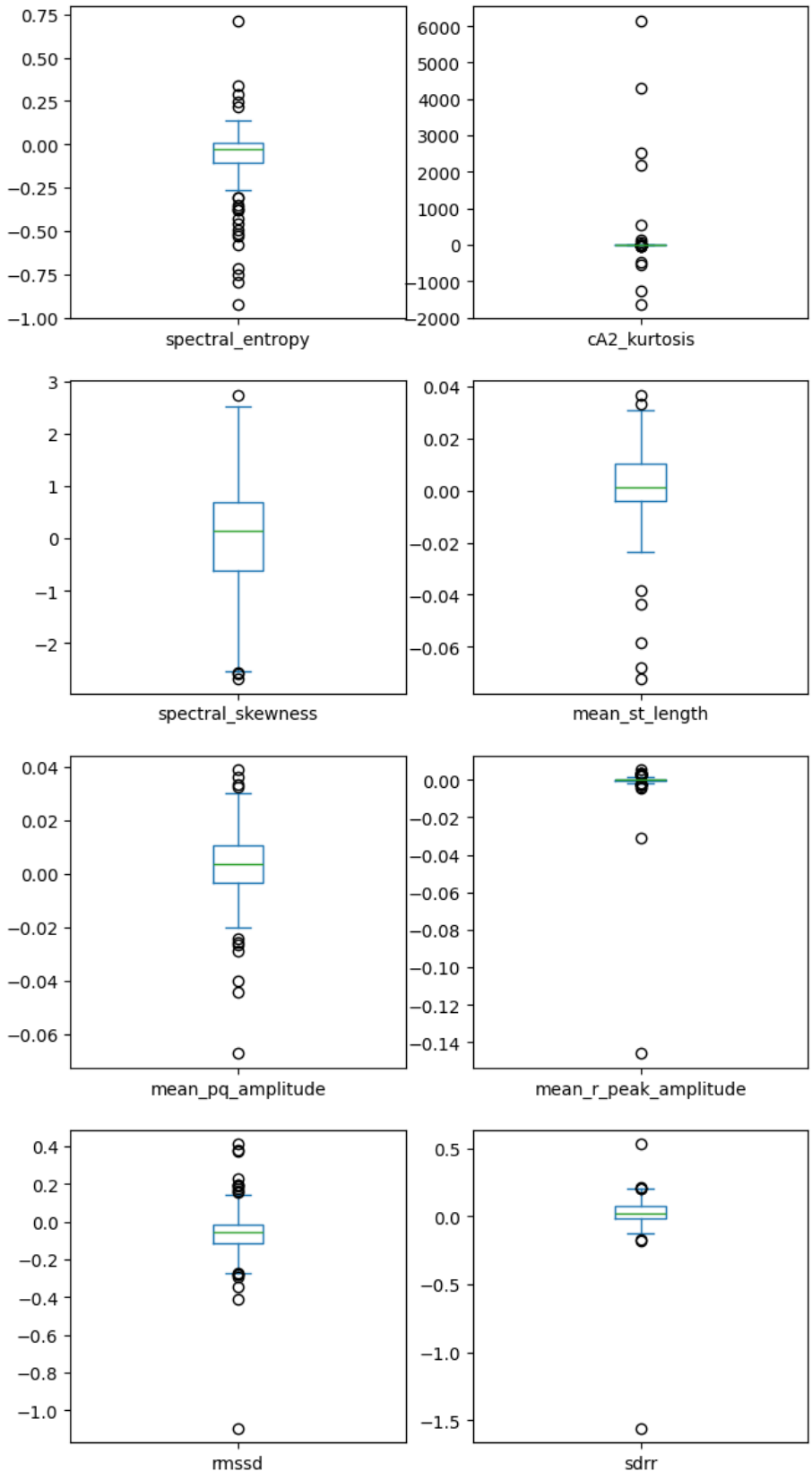

Figure C.2: Box plots of feature differences 2/2